Chemical Engineering Journal 96 (2003) 81–98

Chemical Engineering Journal

www.elsevier.com/locate/cej

Methods for multiphase computational fluid dynamics

B.G.M. van Wachem*, A.E. Almstedt

Department of Thermo and Fluid Dynamics, Chalmers University of Technology, SE-412 96 Gothenburg, Sweden

Dedicated to C.M. van den Bleek for his retirement

Abstract

This paper presents an overview of the physical models for computational fluid dynamic (CFD) predictions of multiphase flows. The governing equations and closure models are derived and presented for fluid–solid flows and fluid–fluid flows, both in an Eulerian and a Lagrangian framework. Some results obtained with these equations are presented. Finally, the capabilities and limitations of multiphase CFD are discussed.

Keywords: Multiphase flow; Computational fluid dynamics

1. Introduction

Multiphase flows are encountered in many processes in industrial operations. Numerous examples can be found in the chemical, petroleum, pharmaceutical, agricultural, biochemical, food, electronic, and power-generation industries. Due to the inherent complexity of multiphase flows, from a physical as well a numerical point of view, "general" applicable computational fluid dynamics (CFD) codes are non-existent. The reasons for the lack of fundamental knowledge on multiphase flows are three-fold:

(1) Multiphase flow is a very complex physical phenomenon where many flow types can occur (gas–solid, gas–liquid, liquid–liquid, etc.) and within each flow type several possible flow regimes can exist (annular flow, jet flow, slug flow, bubbly flow, etc.).
(2) The complex physical laws and mathematical treatment of phenomena occurring in the presence of the two phases (interface dynamics, coalescence, break-up, drag, . . .) are still largely undeveloped. For example, to date there is still no agreement on the governing equations. In addition, proposed constitutive models are empirical but often lack experimental validation for the conditions they are applied under.
(3) The numerics for solving the governing equations and closure laws of multiphase flows are extremely complex. Very often multiphase flows show inherent oscillatory behaviour, requiring costly transient solution algorithms. Almost all CFD codes apply extensions of single-phase solving procedures, leading to diffusive or unstable solutions, and require very short time-steps, or CFL numbers.

In spite of the major difficulties mentioned above, significant progress has been made in various areas of multiphase flow CFD. In their famous article from 1967, Anderson and Jackson [1] derive the continuum equations of motion for gas–particle flow. Garg and co-workers [2,3] perform impressive computations based upon these governing equations, obtaining bubble behaviour in a particle bed. Later, many authors (for instance, [4–20]) improve the constitutive models and/or perform simulations for various gas–solid flows.

In 1975, Ishii [21] derives multiphase fluid–fluid governing equations from first principles, going through the details of the derivation in great detail. The inherent assumptions of this derivation are slightly different from the assumptions applied by Anderson and Jackson [1], which constrain the types of multiphase flow to which they can be applied. Ishii [21] also gives appropriate closure models for various gas–liquid flow conditions.

Up till the early 1980s, most computational models for multiphase flow on an application level describe both the continuous phase and the dispersed phase by a so-called Eulerian model. In these models the dispersed phase, like the continuous phase, is described as a continuous fluid with appropriate closures. Hence, one calculates only the average local volume fraction, velocity, etc. and not the properties of each individual dispersed particle or droplet. This type

* Corresponding author.
E-mail address: berend@tfd.chalmers.se (B.G.M. van Wachem).
URL: http://www.tfd.chalmers.se/∼berend.

1385-8947/$ – see front matter © 2003 Elsevier B.V. All rights reserved.
doi:10.1016/j.cej.2003.08.025

Nomenclature

$\boldsymbol{a}$	acceleration ($m\,s^{-2}$)
$\boldsymbol{c}$	velocity ($m\,s^{-1}$)
$\boldsymbol{C}$	fluctuating velocity ($m\,s^{-1}$)
C	empirical coefficient
C_d	drag coefficient
d	diameter (m)
$\bar{\bar{D}}$	strain rate tensor (s^{-1})
e	coefficient of restitution
f	probability density function
$\boldsymbol{f}$	fluid phase point property
$\boldsymbol{F}$	force ($kg\,m\,s^{-2}$)
Fr	empirical material constant ($N\,m^{-2}$)
$\boldsymbol{g}(r)$	weighting function
$\boldsymbol{g}$	gravitational constant ($m\,s^{-2}$)
$\boldsymbol{g}$	velocity difference ($m\,s^{-1}$)
g_0	radial distriubtion function at particle contact
I	moment of inertia ($kg\,m^2$)
$\boldsymbol{I}$	interphase momentum exchange due to form and viscous drag ($N\,s^{-1}$)
$\boldsymbol{J}$	slip velocity ($m\,s^{-1}$)
$\boldsymbol{J}$	impulse transfer during collision ($kg\,m\,s^{-1}$)
k	stiffness coefficient
L	interfacial area per unit volume (m^{-1})
m	particle mass (kg)
$\boldsymbol{M}$	total interphase momentum exchange ($N\,s^{-1}$)
n	empirical constant in frictional stress
n	number density
$\boldsymbol{n}$	normal vector (m)
p	empirical constant in frictional stress
P	pressure ($N\,m^{-2}$)
$\boldsymbol{P}$	impulse transfer between two particles ($kg\,m\,s^{-1}$)
$\boldsymbol{q}$	relative velocity ($m\,s^{-1}$)
$\boldsymbol{r}$	point in space (m)
t	time (s)
$\boldsymbol{u}$	velocity vector ($m\,s^{-1}$)
U	velocity component ($m\,s^{-1}$)
$\boldsymbol{v}$	velocity vector ($m\,s^{-1}$)
V	velocity component ($m\,s^{-1}$)
V	volume (m^3)
V_r	ratio of terminal velocity of a group of particles to that of an isolated particle
W	velocity component ($m\,s^{-1}$)
$\boldsymbol{x}$	position vector (m)
X	phase indicator

Greek letters

β	interphase drag constant ($kg\,m^{-3}\,s^{-1}$)
γ	dissipation of granular energy ($kg\,m^{-3}s^{-1}$)
γ	angle between impact and normal
δ	particle–particle overlap (m)
ϵ	volume fraction
η	damping coefficient
η	$=\frac{1}{2}(1+e)$
θ	contribution due to particle collisions
Θ	granular temperature ($m^2\,s^{-2}$)
κ	solids thermal conductivity ($kg\,m^{-1}s^{-1}$)
λ	solids bulk viscosity (Pa s)
λ_{mfp}	mean free path (m)
μ	solids shear viscosity (Pa s)
μ	friction coefficient
ξ	color function
ξ	tangential coefficient of restitution
ρ	density ($kg\,m^{-3}$)
σ	particle radius (m)
$\bar{\bar{\sigma}}$	total stress tensor ($N\,m^{-2}$)
$\bar{\bar{\tau}}$	viscous stress tensor ($N\,m^{-2}$)
ϕ	particle property, *any*
ϕ	angle of internal friction
χ	contribution due to particle collisions
ω	rotational velocity (s^{-1})

Subscripts

am	added mass
b	dispersed phase conglomerates (e.g. bubble)
drag	drag
e	external
e	effective
f	frictional
g	gas phase
hist	history
i	interface
j	either phase, not k
k	either phase
kinetic	kinetic theory
lift	lift
min	minimum; kick-in value
max	maximum
p	particle
r	relative
s	solids phase
turb	turbulent
w	wall

of modeling is discussed in Section 2. With the increase of computational power, however, also the Lagrangian formulation of the dispersed phase becomes feasible, but unfortunately the amount of dispersed particles or droplets that can be tracked is, even today and in the near future, very limited. However, specific features of gas–fluid or droplet–fluid flow can be effectively studied [22–25]. This is discussed in in Section 3.

A separate class of methods to track interfaces in fluid–fluid flow are volume-of-fluid (VOF), level-set or front tracking methods. Although the idea behind these methods is similar, their numerical implementation, and thus behaviour,

may differ greatly. These methods describe both fluids with one set of equations and solve another equation for the evolution of the interfaces between the two fluids. The equation prescribing the evolution of the interface may be formulated in a Eulerian framework [26–28] or in a Lagrangian framework [29,30] or in a combination of both [31]. These types of models are described in Section 4.

2. Eulerian–Eulerian modeling

Many authors propose governing equations without citing, or incorrectly citing, a reference for the basis or derivation of the equations they employ. There are a number of sources for the derivation of governing equations for multiphase systems, but the inherent assumptions in the different derivations constrain the types of multiphase flow to which they can be applied. There is a lot of research on the closure models for these governing equations. Here, we give a short derivation and overview of the governing equations for various types of multiphase flows.

2.1. Fluid–fluid flows

2.1.1. Governing equations

In a fluid–fluid formulation, both phases can be averaged over a fixed volume, cf. Ishii [21]. This volume is relatively large compared to the size of individual molecules. A phase indicator function is introduced, $X_k(\boldsymbol{r})$, which is unity when the point $\boldsymbol{r}$ is occupied by phase k, and zero if it is not. Averaging over this function leads to the volume fraction of both phases,

$$\epsilon_k = \frac{1}{V}\int_V X_k(\boldsymbol{r})\mathrm{d}V_\mathrm{r} \tag{1}$$

where V is the averaging volume. Since both the continuous and dispersed phases are liquids, they are treated in the same way in the averaging process. Hence, the momentum balances for both phases are the same,

$$\frac{\partial \epsilon_k \rho_k \langle \boldsymbol{v}_k\rangle}{\partial t} + \nabla(\epsilon_k \rho_k \langle \boldsymbol{v}_k\rangle\langle \boldsymbol{v}_k\rangle) = -\nabla\cdot(\epsilon_k\langle P_k\rangle) + \nabla\cdot(\epsilon_k\langle\bar{\bar{\tau}}_k\rangle) + \epsilon_k\rho_k\boldsymbol{g} + \boldsymbol{M}_k \tag{2}$$

where k is the phase number and $\boldsymbol{M}_k$ is the interphase momentum exchange between the phases, with $\sum_i \boldsymbol{M}_i = 0$. The density terms ρ_k are averaged in the same way as the velocity. The distribution of stress within both phases is important since the dispersed phase is considered as a fluid. Hence, "jump" conditions are used to determine $\boldsymbol{M}_k$. The interphase momentum transfer is defined as

$$\begin{aligned}\boldsymbol{M}_k &= -\sum_j \frac{1}{L_j}(P_k\boldsymbol{n}_k - \boldsymbol{n}_k\cdot\bar{\bar{\tau}}_k)\\ &= \sum_j \frac{1}{L_j}[(\langle P_{ki}\rangle - P_k)\boldsymbol{n}_k - \langle P_{ki}\rangle\boldsymbol{n}_k - \boldsymbol{n}_k\cdot(\langle\bar{\bar{\tau}}_{ki}\rangle - \bar{\bar{\tau}}_k) + \boldsymbol{n}_k\cdot\langle\bar{\bar{\tau}}_{ki}\rangle]\end{aligned} \tag{3}$$

Table 1
The governing equations for fluid–fluid and fluid–solid flows

Continuity equations (equal for both phases)

$$\frac{\partial\epsilon}{\partial t} + \nabla(\epsilon\boldsymbol{v}) = 0$$

Momentum equations for fluid–solid flow

$$\rho_\mathrm{g}\epsilon_\mathrm{g}\left[\frac{\partial\boldsymbol{v}_\mathrm{g}}{\partial t} + \boldsymbol{v}_\mathrm{g}\cdot\nabla\boldsymbol{v}_\mathrm{g}\right] = -\epsilon_\mathrm{g}\nabla P + \epsilon_\mathrm{g}\nabla\cdot\bar{\bar{\tau}}_\mathrm{g} + \epsilon_\mathrm{g}\rho_\mathrm{g}\boldsymbol{g} - \boldsymbol{I}$$

$$\rho_\mathrm{s}\epsilon_\mathrm{s}\left[\frac{\partial\boldsymbol{v}_\mathrm{s}}{\partial t} + \boldsymbol{v}_\mathrm{s}\cdot\nabla\boldsymbol{v}_\mathrm{s}\right] = -\epsilon_\mathrm{s}\nabla P + \epsilon_\mathrm{s}\nabla\cdot\bar{\bar{\tau}}_\mathrm{g} + \nabla\cdot\bar{\bar{\tau}}_\mathrm{s} - \nabla P_\mathrm{s} + \epsilon_\mathrm{s}\rho_\mathrm{s}\boldsymbol{g} + \boldsymbol{I}$$

Momentum equations for fluid–fluid flow

$$\rho_i\epsilon_i\left[\frac{\partial\boldsymbol{v}_i}{\partial t} + \boldsymbol{v}_i\cdot\nabla\boldsymbol{v}_i\right] = -\epsilon_i\nabla P + \nabla\cdot\epsilon_i\bar{\bar{\tau}}_i + \epsilon_i\rho_i\boldsymbol{g} - \boldsymbol{I}$$

$$\rho_j\epsilon_j\left[\frac{\partial\boldsymbol{v}_j}{\partial t} + \boldsymbol{v}_j\cdot\nabla\boldsymbol{v}_j\right] = -\epsilon_j\nabla P + \nabla\cdot\epsilon_j\bar{\bar{\tau}}_j + \epsilon_j\rho_j\boldsymbol{g} + \boldsymbol{I}$$

where $1/L_j$ is the interfacial area per unit volume, P_k is the pressure in the bulk of phase k, $\langle P_{ki}\rangle$ is the average pressure of phase k at the interface, $\bar{\bar{\tau}}_k$ the shear stress in the bulk, and $\langle\bar{\bar{\tau}}_{ki}\rangle$ represents the average shear stress at the interface. Mass transfer between the phases is not assumed. The terms $(\langle P_{ki}\rangle - P_k)\boldsymbol{n}_k$ and $\boldsymbol{n}_k(\langle\bar{\bar{\tau}}_{ki}\rangle - \bar{\bar{\tau}}_k)$ are identified by Ishii [21] as the form drag and the viscous drag, respectively, making up the total drag force. The other terms can be written out as

$$\boldsymbol{M}_k = \boldsymbol{I} + \langle P_k\rangle\nabla\epsilon_k + (\langle P_{ki}\rangle - \langle P_k\rangle)\nabla\epsilon_k - (\nabla\epsilon_k)\cdot\langle\bar{\bar{\tau}}_{ki}\rangle \tag{4}$$

where $\boldsymbol{I}$ represents the total form and viscous drag. According to Ishii and Mishima [32], the last term on the right hand side is an interfacial shear term which is important in a separated flow. According to Ishii [21], the term $(\langle P_{ki}\rangle - \langle P_k\rangle)$ only plays a role when the pressure at the bulk is significantly different from that at the interface as in stratified flows. For many applications both terms are negligible, and

$$\boldsymbol{M}_k = \boldsymbol{I} + \langle P_k\rangle\nabla\epsilon_k \tag{5}$$

The final resulting governing equations are shown in Table 1.

2.1.2. Closure models

In the Euler–Euler concept, sometimes called the two-fluid approach, both the continuous and dispersed phases are considered as continuous media. These models incorporate two-way coupling, which is especially important for high voidage flows. A drawback of these models is, however, that they need complex closure relations.

The interfacial momentum transfer between the liquid and the gas includes a number of force contributions,

$$\boldsymbol{I} = \boldsymbol{I}_\mathrm{drag} + \boldsymbol{I}_\mathrm{am} + \boldsymbol{I}_\mathrm{hist} + \boldsymbol{I}_\mathrm{turb} + \boldsymbol{I}_\mathrm{lift} \tag{6}$$

where $\boldsymbol{I}_\mathrm{drag}$ denotes the form and viscous drag, $\boldsymbol{I}_\mathrm{am}$ denotes the added mass force which is an inertial force caused by relative acceleration, $\boldsymbol{I}_\mathrm{hist}$ is the history or Basset force, which is a viscous force caused by relative acceleration, $\boldsymbol{I}_\mathrm{turb}$ denotes the effect of turbulent fluctuations on the effective momentum transfer, and $\boldsymbol{I}_\mathrm{lift}$ is the lift force which denotes the

transverse force caused by rotational strain, velocity gradients, or the presence of walls [9].

The drag force represents the mean interphase momentum transfer coming from the local perturbations induced by the dispersed phase

$$\boldsymbol{I}_{\mathrm{drag}} = \epsilon_j \rho_j \left\langle \frac{\rho_k}{\rho_j} \frac{3}{4} \frac{C_{\mathrm{d}}}{d_{\mathrm{b}}} |\boldsymbol{v}_{\mathrm{r}}| \boldsymbol{v}_{\mathrm{r}} \right\rangle \tag{7}$$

where d_{b} is the average size of the dispersed phase conglomerates (e.g. bubbles), C_{d} the drag coefficient [33], and $\boldsymbol{v}_{\mathrm{r}}$ is the local relative velocity between the dispersed phase and the surrounding fluid flow. This expression for the drag is valid for relative dilute systems. As the dispersed fraction increases, the effect of mutual hindrance between the dispersed phase conglomerates plays an increasing role, and this effect is not taken into account. Expressions to determine the drag at high dispersed phase fractions are highly empirical of nature and applicable to a limited number of systems [34].

The added mass force takes into account the inertial forces due to the relative acceleration between the phases. A general equation for this force is given by

$$\boldsymbol{I}_{\mathrm{am}} = \epsilon_j \rho_k C_{\mathrm{am}} \left(\frac{D_k \boldsymbol{v}_k}{Dt} - \frac{D_j \boldsymbol{v}_j}{Dt} \right) \tag{8}$$

where the added mass coefficient, C_{am}, is a function of the volume fraction [35].

The history force is a viscous force due to the relative acceleration between the two phases. Most often, this force is ignored in continuum modelling, and there is not even full agreement of its formulation even for the single bubble case [34]. Drew and Lahey [36] give an expression for the history force combined with the lift force,

$$\boldsymbol{I}_{\mathrm{hist}} = \frac{9}{d_p} \epsilon_k \sqrt{\frac{\rho_j \mu_j}{\pi}} \int_0^t \frac{\boldsymbol{a}(\boldsymbol{r}, t)}{\sqrt{t - \tau}} \, \mathrm{d}\tau \tag{9}$$

where the appropriate frame-indifferent acceleration, according to [36], is given by

$$\boldsymbol{a}(\boldsymbol{r}, t) = \left(\frac{D_j \boldsymbol{u}_j}{Dt} - \frac{D_j \boldsymbol{u}_j}{Dt} \right) - (\boldsymbol{u}_j - \boldsymbol{u}_j) \times (\nabla \times \boldsymbol{u}_j) \tag{10}$$

The effect of turbulence on interphase momentum transfer is largely unknown. An important turbulent effect comes in the form and viscous drag. The relative velocity, $\boldsymbol{v}_{\mathrm{r}}$, in this equation should contain the averages of fluctuating velocity, sometimes referred by as the turbulent drift velocity [5]. This type of models typically leads to dispersive forces ($\sim \nabla \epsilon_j$).

The lift force represents the transverse force due to rotational strain, velocity gradients, or the presence of walls. A general equation for the lift force caused by rotational strain is given by

$$\boldsymbol{I}_{\mathrm{lift,r}} = \epsilon_j \rho_i C_{\mathrm{li,r}} (\boldsymbol{v}_j - \boldsymbol{v}_i) \times \boldsymbol{\Omega} \tag{11}$$

and the equation for the lift force caused by velocity gradients is given by

$$\boldsymbol{I}_{\mathrm{lift},v} = \epsilon_j \rho_i C_{\mathrm{li,v}} (\boldsymbol{v}_j - \boldsymbol{v}_i) \times (\nabla \times \boldsymbol{v}_i) \tag{12}$$

where $C_{\mathrm{li,r}}$ and $C_{\mathrm{li,v}}$ are the lift force coefficients associated with rotational strain and velocity gradients, respectively. From laminar, inviscid flow the value of 1/2 can be determined for the lift force coefficient for rotational strain. In literature, a wide range of values can be found for the lift force coefficient, as the above equations originates from inviscid flow around a single sphere. Tomiyama et al. [37] have performed experiments of single bubbles in simple shear flows and have found positive and negative values for the lift force coefficient, depending upon the specific bubble characteristics. According to Lathouwers [34] the lift force coefficient in multiple bubble modelling is sometimes used to correct for other effects unaccounted for by present models.

2.2. Fluid–solid flows

2.2.1. Governing equations

Anderson and Jackson [1] and Jackson [38,39] use a formal mathematical definition of local mean variables to translate the point Navier–Stokes equations for the fluid and the Newton's equation of motion for a single particle directly into continuum equations representing momentum balances for the fluid and solid phases. The point variables are averaged over regions large with respect to the particle diameter but small with respect to the characteristic dimension of the complete system. A weighting function, $g(|\boldsymbol{x} - \boldsymbol{y}|)$, is introduced in forming the local averages of system point variables, where $|\boldsymbol{x} - \boldsymbol{y}|$ denotes the separation of two arbitrary points in space. The integral of g over the total space is normalized to unity:

$$4\pi \int_0^\infty g(r) r^2 \, \mathrm{d}r = 1 \tag{13}$$

The 'radius' l of function g is defined by

$$\int_0^l g(r) r^2 \, \mathrm{d}r = \int_l^\infty g(r) r^2 \, \mathrm{d}r \tag{14}$$

Provided g is chosen so that l satisfies $a \ll l \ll L$, where a is the particle radius and L is the shortest macroscopic length scale, averages defined should not depend significantly on the particular functional form of g or its radius.

The gas-phase volume fraction $\epsilon_{\mathrm{g}}(\boldsymbol{x})$ and the particle number density $n(\boldsymbol{x})$ at point $\boldsymbol{x}$ are directly related to the weighting function g:

$$\epsilon_{\mathrm{g}}(\boldsymbol{x}) = \int_{V_{\mathrm{g}}} g(|\boldsymbol{x} - \boldsymbol{y}|) \, \mathrm{d}V_y \tag{15}$$

$$n(\boldsymbol{x}) = \sum_p g(|\boldsymbol{x} - \boldsymbol{x}_p|) \tag{16}$$

where V_{g} is the fluid phase volume, and $\boldsymbol{x}_p$ is the position of the center of particle p. The local mean value of the fluid phase point properties, $\langle \boldsymbol{f} \rangle_{\mathrm{g}}$ is defined by

$$\epsilon_{\mathrm{g}}(\boldsymbol{x}) \langle \boldsymbol{f} \rangle_{\mathrm{g}}(\boldsymbol{x}) = \int_{V_{\mathrm{g}}} \boldsymbol{f}(\boldsymbol{y}) g(|\boldsymbol{x} - \boldsymbol{y}|) \, \mathrm{d}V_y \tag{17}$$

The solid-phase averages are not defined analogous to the continuous fluid phase averages since the motion of the solid phase is determined with respect to the center of the particle and average properties need only depend on the properties of the particle as a whole. Hence, the local mean value of the solid-phase point properties is defined by

$$n(\boldsymbol{x})\langle \boldsymbol{f}\rangle_{\mathrm{s}}(\boldsymbol{x}) = \sum_p \boldsymbol{f}_{\mathrm{s}} g(|\boldsymbol{x}-\boldsymbol{x}_p|) \tag{18}$$

The average space and time derivatives for the fluid and solid phases follow from the above definitions. The averaging rules are then applied to the point continuity and momentum balances for the fluid. For the solid phase, the averaging rules are applied to the equation of motion of a single particle p:

$$\rho_{\mathrm{s}} V_p \frac{\partial \boldsymbol{v}_{\mathrm{s}}}{\partial t} = \int_{S_p} \bar{\bar{\sigma}}_{\mathrm{g}}(\boldsymbol{y})\boldsymbol{n}(\boldsymbol{y})\,\mathrm{d}s_y + \sum_{q\neq p} \boldsymbol{f}_{qp} + \rho_{\mathrm{s}} V_p \boldsymbol{g} \tag{19}$$

where $\boldsymbol{v}_{\mathrm{s}}$ is the particle velocity, ρ_{s} is the particle density, V_p is the volume of particle p, $\bar{\bar{\sigma}}_{\mathrm{g}}$ is the gas-phase stress tensor, S_p denotes the surface of particle p, and $\boldsymbol{f}_{qp}$ represents the resultant force exerted on the particle p from contacts with other particles.

The resulting momentum balances for the fluid and solid phases, dropping the averaging brackets $\langle\,\rangle$ on the variables, are as follows:

$$\rho_{\mathrm{g}}\epsilon_{\mathrm{g}}\left[\frac{\partial}{\partial t}\boldsymbol{v}_{\mathrm{g}} + \boldsymbol{v}_{\mathrm{g}}\cdot\nabla\boldsymbol{v}_{\mathrm{g}}\right] = \nabla(\epsilon_{\mathrm{g}}\bar{\bar{\sigma}}_{\mathrm{g}}) - \sum_p \int_{S_p} \bar{\bar{\sigma}}_{\mathrm{g}}\cdot\boldsymbol{n}(\boldsymbol{y})g|\boldsymbol{x}-\boldsymbol{y}|\,\mathrm{d}s_y + \rho_{\mathrm{g}}\epsilon_{\mathrm{g}}\boldsymbol{g} \tag{20}$$

$$\rho_{\mathrm{s}}\epsilon_{\mathrm{s}}\left[\frac{\partial}{\partial t}\boldsymbol{v}_{\mathrm{s}} + \boldsymbol{v}_{\mathrm{s}}\cdot\nabla\boldsymbol{v}_{\mathrm{s}}\right] = \sum_p g|\boldsymbol{x}-\boldsymbol{x}_p|\int_{S_p}\bar{\bar{\sigma}}_{\mathrm{g}}\boldsymbol{n}(\boldsymbol{y})\,\mathrm{d}s_y + \nabla\cdot\bar{\bar{\sigma}}_{\mathrm{s}} + \rho_{\mathrm{s}}\epsilon_{\mathrm{s}}\boldsymbol{g} \tag{21}$$

The first term on the right hand side of the gas phase equation of motion represents the effect of stresses in the gas phase, the second term on the right hand side represents the traction exerted on the gas phase by the particle surfaces, and the third term represents the gravity force on the fluid. The first term on the right hand side of the solid-phase equation of motion represents the forces exerted on the particles by the fluid, the second term on the right hand side represents the force due to solid-solid contacts, which can be described using concepts from kinetic theory, and the third term represents the gravity force on the particles. The averaged shear tensor of the gas phase can be rewritten with the Newtonian definition as

$$\bar{\bar{\sigma}}_{\mathrm{g}} = -P_{\mathrm{g}}\bar{\bar{I}} + \frac{\mu_{\mathrm{g}}}{\epsilon_{\mathrm{g}}}(\nabla\boldsymbol{v}_{\mathrm{g}} + (\nabla\boldsymbol{v}_{\mathrm{g}})^{\mathrm{T}}) \tag{22}$$

where the gas phase volume fraction is introduced in the volume averaging process.

Note that the forces due to fluid traction are treated differently in the fluid- and solid-phase momentum balances. In the particle phase, only the resultant force acting on the center of the particle is relevant; the distribution of stress within each particle is not needed to determine its motion. Hence, in the solid-phase momentum balance, the resultant forces due to fluid traction acting everywhere on the surface of the particles are calculated first, then these are averaged to the particle centers. In the fluid-phase momentum balance, the traction forces fluid–solid interaction are calculated at the particle surface, and are employed there. Hence, the fluid-phase traction term is given as

$$\sum_p \int_{S_p} \bar{\bar{\sigma}}_{\mathrm{g}}\cdot\boldsymbol{n}(\boldsymbol{y})g|\boldsymbol{x}-\boldsymbol{y}|\,\mathrm{d}s_y = \sum_p g|\boldsymbol{x}-\boldsymbol{x}_p|\int_{S_p}\bar{\bar{\sigma}}_{\mathrm{g}}\cdot\boldsymbol{n}(\boldsymbol{y})\,\mathrm{d}s_y - \nabla\left[a\sum_p g|\boldsymbol{x}-\boldsymbol{x}_p|\int_{S_p}(\bar{\bar{\sigma}}_{\mathrm{g}}\cdot\boldsymbol{n}(\boldsymbol{y}))\boldsymbol{n}(\boldsymbol{y})\,\mathrm{d}s_y\right] + \mathrm{O}(\nabla^2) \tag{23}$$

which is a result of a Taylor series expansion in $g|\boldsymbol{x}-\boldsymbol{y}|$ about the center of the particle with radius a. Here, terms of $\mathrm{O}(\nabla^2)$ and higher have been neglected. Note that the first term on the right hand side of Eq. (23) is the same as the fluid traction term in the particle-phase momentum balance. The difference in the manner in which the resultant forces due to fluid traction act on the surfaces of the particles is a key distinction between the Jackson (see Eq. (23)) and Ishii (Eq. (3)) formulations. In the Ishii [21] formulation, applicable to fluid droplets, the fluid-droplet traction term is the same in the gas phase and the dispersed phase governing equations.

The integrals involving the traction on a particle surface have been derived by [40] and are given in [38]

$$\sum_p g|\boldsymbol{x}-\boldsymbol{x}_p|\int_{S_p}\bar{\bar{\sigma}}_{\mathrm{g}}\cdot\boldsymbol{n}(\boldsymbol{y})\,\mathrm{d}s_y = \frac{\boldsymbol{I}}{\epsilon_{\mathrm{s}}} + \rho_{\mathrm{g}}\epsilon_{\mathrm{s}}\boldsymbol{g} + \rho_{\mathrm{g}}\epsilon_{\mathrm{s}}\frac{D_{\mathrm{g}}\boldsymbol{v}_{\mathrm{g}}}{Dt} \tag{24}$$

$$\nabla\left[a\sum_p g|\boldsymbol{x}-\boldsymbol{x}_p|\int_{S_p}(\bar{\bar{\sigma}}_{\mathrm{g}}\cdot\boldsymbol{n}(\boldsymbol{y}))\boldsymbol{n}(\boldsymbol{y})\,\mathrm{d}s_y\right] = -\nabla(\epsilon_{\mathrm{s}}P_{\mathrm{g}}) \tag{25}$$

where $\boldsymbol{I}$ is the interphase momentum transfer coefficient, including viscous and form drag, lift force, etc. The final governing equations are presented in Table 1.

Comparing the fluid–fluid and fluid–solid momentum balances from Table 1, the differences are two-fold. First, in the fluid–solid case, the solid volume fraction multiplied by the gradient of the total gas-phase stress tensor in included in the solid-phase momentum balance. In the fluid–fluid case, only the solid volume fraction multiplied by the gradient

of the pressure is included. Secondly, in the fluid–fluid approach in the gas-phase momentum balance, the pressure carries the gas volume fraction outside the gradient operator; the shear stress carries the gas volume fraction inside the gradient operator. In the fluid–solid approach both stresses are treated equally with respect to the gas volume fraction and the gradient operators. When the gas phase shear stress plays an important role, these differences may be significant near large gradients of volume fraction, i.e. near interfaces. Some authors employ liquid–liquid governing equations to describe gas–solid flows (for instance [4,9]) and the impact of the discrepancy between the two sets of governing equations depends upon the application [20].

2.2.2. Closure models

2.2.2.1. Interphase momentum transfer. In dilute flows, the interphase momentum transfer due to form and viscous drag is modelled with a model after the drag on a single particle in an infinite fluid, with the same equation as in fluid–fluid flow:

$$\boldsymbol{I}_{\text{drag}} = \epsilon_{\text{s}}\rho_{\text{g}}\left\langle \frac{\rho_{\text{g}}}{\rho_{\text{s}}}\frac{3}{4}\frac{C_{\text{d}}}{d_p}|\boldsymbol{v}_{\text{r}}|\boldsymbol{v}_{\text{r}}\right\rangle \tag{26}$$

where C_{d} is the drag coefficient [33,41], d_p is the average local particle diameter, and $\boldsymbol{v}_{\text{r}}$ is the relative local velocity between the fluid and the solid phase. Although most authors take this relative velocity as the difference of the local fluid and the solid velocities, this is formally not correct; the undisturbed turbulent fluid velocity should be used instead. This is discussed later on.

In more dense flows, the form drag and viscous drag are generally combined in one empirical parameter, the interphase drag constant β, in the modeling of the momentum transfer between the two phases. The interphase momentum transfer is then written as

$$\boldsymbol{I}_{\text{drag}} = \beta\boldsymbol{v}_{\text{r}} \tag{27}$$

The drag coefficient β is typically obtained experimentally from pressure drop measurements in fixed, fluidized, or settling beds, or by volume fraction dependent sedimentation experiments [42]. Ergun [43] performed measurements in fixed liquid–solid beds at packed conditions to determine the pressure drop. Based upon this model, Gidaspow [12] proposed the drag model:

$$\beta = \begin{cases} 150\dfrac{\epsilon_{\text{s}}^2\mu_{\text{g}}}{(1-\epsilon_{\text{s}})d_{\text{s}}^2} + \dfrac{7}{4}\dfrac{\epsilon_{\text{s}}\rho_{\text{g}}|\boldsymbol{v}_{\text{g}}-\boldsymbol{v}_{\text{s}}|}{d_{\text{s}}}, & \text{if } \epsilon_{\text{s}} > 0.2 \\ \dfrac{3}{4}C_{\text{d}}\dfrac{(1-\epsilon_{\text{s}})\epsilon_{\text{s}}\rho_{\text{g}}|\boldsymbol{v}_{\text{g}}-\boldsymbol{v}_{\text{s}}|}{d_{\text{s}}}(1-\epsilon_{\text{s}})^{-2.65}, & \text{if } \epsilon_{\text{s}} \le 0.2 \end{cases} \tag{28}$$

Wen and Yu [44] have performed settling experiments of solid particles in a liquid over a wide range of solid volume fractions and have correlated their data and that of others for solids concentrations applying the Richardson and Zaki correction factor [42]. $0.01 \le \epsilon_{\text{s}} \le 0.63$:

$$\beta = \frac{3}{4}C_{\text{d}}\frac{(1-\epsilon_{\text{s}})\epsilon_{\text{s}}\rho_{\text{g}}|\boldsymbol{v}_{\text{g}}-\boldsymbol{v}_{\text{s}}|}{d_{\text{s}}}(1-\epsilon_{\text{s}})^{-2.65} \tag{29}$$

Both equations lead to similar results [20].

2.2.2.2. Kinetic theory of granular flow. When the governing equations derived in the previous section are used to predict the behaviour of fluid–solid flows, closures are required. Closure of the solid-phase momentum equation requires a description for the solid-phase stress. When collisional interactions play an important role in the motion of the particles, concepts from kinetic gas theory [45] can be used to describe the effective stresses in the solid phase resulting from particle streaming (kinetic contribution) and direct collisions (collisional contribution). Constitutive relations for the solid-phase stress based on kinetic theory concepts have been derived by Lun et al. [46] allowing for the inelastic nature of particle collisions.

The derivation of the closures start with the Boltzmann description of a mixture of particles. The distribution of velocities among a large number of particles in a volume element $\mathrm{d}\boldsymbol{r}$ can be represented by the distribution of their velocity points $\boldsymbol{c}$ in the velocity space. The number density of this volume element will generally be a function of the location in space, $\boldsymbol{r}$, of the time, t, as well of the velocity $\boldsymbol{c}$. Therefore, the number density of the particles at volume $\boldsymbol{r}$ with velocity $\boldsymbol{c}$ at time t is denoted by $f(\boldsymbol{c}, \boldsymbol{r}, t)$. This definition implies that the probable number of particles which at time t are situated in the volume element $(\boldsymbol{r}, \boldsymbol{r}+\mathrm{d}\boldsymbol{r})$, and have velocities lying in the range $(\boldsymbol{c}, \boldsymbol{c}+\mathrm{d}\boldsymbol{c})$ is $f(\boldsymbol{c}, \boldsymbol{r}, t)\,\mathrm{d}\boldsymbol{c}\,\mathrm{d}\boldsymbol{r}$, where f is called the *probability density function.*

We consider particles in which each particle is subject to an external force with acceleration $\boldsymbol{a}$. Between times t and $t+\mathrm{d}t$ the velocity $\boldsymbol{c}$ of any particle that does not collide with another particle will change to $\boldsymbol{c}+\boldsymbol{a}\,\mathrm{d}t$, and its position vector $\boldsymbol{r}$ will change to $\boldsymbol{r}+\boldsymbol{c}\,\mathrm{d}t$. The number of particles $f(\boldsymbol{c}, \boldsymbol{r}, t)\,\mathrm{d}\boldsymbol{c}\,\mathrm{d}\boldsymbol{r}$ at time t is equal to the number of particles $f(\boldsymbol{c}+\boldsymbol{a}\,\mathrm{d}t, \boldsymbol{r}+\boldsymbol{c}\,\mathrm{d}t, t+\mathrm{d}t)\,\mathrm{d}\boldsymbol{c}\,\mathrm{d}\boldsymbol{r}$ if collisions between particles are neglected. The change in f over $\mathrm{d}t$ is caused only by collisions of particles:

$$\{f(\boldsymbol{c}+\boldsymbol{a}\,\mathrm{d}t, \boldsymbol{r}+\boldsymbol{c}\,\mathrm{d}t, t+\mathrm{d}t) - f(\boldsymbol{c}, \boldsymbol{r}, t)\}\,\mathrm{d}\boldsymbol{c}\,\mathrm{d}\boldsymbol{r} = \frac{\partial_{\text{e}} f}{\partial t}\,\mathrm{d}\boldsymbol{c}\,\mathrm{d}\boldsymbol{r}\,\mathrm{d}t \tag{30}$$

where $\partial_{\text{e}} f/\partial t$ is the rate of change of f at a fixed point due to particle collisions. By dividing by $\mathrm{d}\boldsymbol{c}\mathrm{d}\boldsymbol{r}\,\mathrm{d}t$ and making dt tend to zero, Boltzmann's equation for f is obtained:

$$\frac{\partial f}{\partial t} + \boldsymbol{c}\cdot\nabla f + \boldsymbol{a}\frac{\partial f}{\partial \boldsymbol{c}} = \frac{\partial_{\text{e}} f}{\partial t} \tag{31}$$

or

$$\mathcal{D}f = \frac{\partial_{\text{e}} f}{\partial t} \tag{32}$$

where $\mathcal{D}f$ denotes the left hand side of Eq. (31).

Now, let ϕ be any particle property. If the Boltzmann equation is multiplied by $\phi \mathrm{d}\boldsymbol{c}$ and integrated over the velocity-space, the equation of change of particle properties is obtained:

$$\int \phi \mathcal{D} f \,\mathrm{d}\boldsymbol{c} = n\mathbb{C}(\phi) \tag{33}$$

in which the right hand term denotes the influence of binary, instantaneous collisions, so it is the integrated form of $\partial_{\mathrm{e}} f/\partial t$. For convenience, the fluctuating velocity $\boldsymbol{C}$ is used as an independent variable instead of $\boldsymbol{c}$:

$$\boldsymbol{C} \equiv \boldsymbol{c} - \langle \boldsymbol{c} \rangle \tag{34}$$

The dependency of f should also be changed to $\boldsymbol{C}$, for example, for $\partial f(\boldsymbol{C})/\partial t$

$$\begin{aligned}\frac{\partial f(\boldsymbol{c} - \langle \boldsymbol{c} \rangle)}{\partial t} &= \frac{\partial f}{\partial \boldsymbol{C}} \frac{\partial \boldsymbol{C}}{\partial t} = \frac{\partial f}{\partial \boldsymbol{C}} \frac{\partial (\boldsymbol{c} - \langle \boldsymbol{c} \rangle)}{\partial t} \\ &= -\frac{\partial \langle \boldsymbol{c} \rangle}{\partial t} \frac{\partial f}{\partial \boldsymbol{C}} + \frac{\partial f}{\partial t} \frac{\partial \boldsymbol{c}}{\partial \boldsymbol{C}}\end{aligned} \tag{35}$$

Hence, $\partial f/\partial t$ and $\partial f/\partial \boldsymbol{r}$ have to be replaced by, respectively,

$$\frac{\partial f}{\partial t} - \frac{\partial \langle \boldsymbol{c} \rangle}{\partial t} \frac{\partial f}{\partial \boldsymbol{C}} \quad \text{and} \quad \frac{\partial f}{\partial \boldsymbol{r}} - \frac{\partial \langle \boldsymbol{c} \rangle}{\partial \boldsymbol{r}} \frac{\partial f}{\partial \boldsymbol{C}}$$

in order to take account of the dependence of f on t and $\boldsymbol{r}$ through the dependence of $\boldsymbol{C}$ on $\boldsymbol{c}$. Hence, the expression for $\mathcal{D} f$ becomes

$$\frac{\partial f}{\partial t} - \frac{\partial \langle \boldsymbol{c} \rangle}{\partial t} \frac{\partial f}{\partial \boldsymbol{C}} + (\langle \boldsymbol{c} \rangle + \boldsymbol{C}) \left(\frac{\partial f}{\partial \boldsymbol{r}} - \frac{\partial \langle \boldsymbol{c} \rangle}{\partial \boldsymbol{r}} \frac{\partial f}{\partial \boldsymbol{C}} \right) + \boldsymbol{a} \frac{\partial f}{\partial \boldsymbol{C}} \tag{36}$$

Now the 'mobile operator' or 'time-derivative following the motion' is introduced as

$$\frac{D}{Dt} = \frac{\partial}{\partial t} + \langle \boldsymbol{c} \rangle \frac{\partial}{\partial \boldsymbol{r}}$$

This is the time derivative following the mean flow. Then

$$\mathcal{D} f = \frac{Df}{Dt} + \boldsymbol{C} \frac{\partial f}{\partial \boldsymbol{r}} + \boldsymbol{a} \frac{\partial f}{\partial \boldsymbol{C}} - \frac{D\langle \boldsymbol{c} \rangle}{Dt} \frac{\partial f}{\partial \boldsymbol{C}} - \frac{\partial f}{\partial \boldsymbol{C}} \boldsymbol{C} : \frac{\partial \langle \boldsymbol{c} \rangle}{\partial \boldsymbol{r}} \tag{37}$$

With this, Eq. (33) can be rewritten into

$$\begin{aligned}&\int \phi \left(\frac{Df}{Dt} + \boldsymbol{C} \frac{\partial f}{\partial \boldsymbol{r}} + \boldsymbol{a} \frac{\partial f}{\partial \boldsymbol{C}} - \frac{D\langle \boldsymbol{c} \rangle}{Dt} \frac{\partial f}{\partial \boldsymbol{C}} - \frac{\partial f}{\partial \boldsymbol{C}} \boldsymbol{C} : \frac{\partial \langle \boldsymbol{c} \rangle}{\partial \boldsymbol{r}} \right) \mathrm{d}\boldsymbol{C} \\ &\quad = n\mathbb{C}(\phi)\end{aligned} \tag{38}$$

For further development of this equation, the following integrals are used for the transformation:

$$\begin{aligned}\int \phi \frac{Df}{Dt} \,\mathrm{d}\boldsymbol{C} &= \frac{D}{Dt} \int \phi f \,\mathrm{d}\boldsymbol{C} - \int \frac{D\phi}{Dt} f \,\mathrm{d}\boldsymbol{C} \\ &= \frac{D(n\langle \phi \rangle)}{Dt} - n \left\langle \frac{D\phi}{Dt} \right\rangle\end{aligned} \tag{39}$$

$$\begin{aligned}\int \phi \boldsymbol{C} \frac{\partial f}{\partial \boldsymbol{r}} \,\mathrm{d}\boldsymbol{C} &= \frac{\partial}{\partial \boldsymbol{r}} \cdot \int \phi \boldsymbol{C} f \,\mathrm{d}\boldsymbol{C} - \int \frac{\partial \phi}{\partial \boldsymbol{r}} \cdot \boldsymbol{C} f \,\mathrm{d}\boldsymbol{C} \\ &= \frac{\partial n\langle \phi \boldsymbol{C} \rangle}{\partial \boldsymbol{r}} - n \left\langle \boldsymbol{C} \frac{\partial \phi}{\partial \boldsymbol{r}} \right\rangle\end{aligned} \tag{40}$$

$$\int \phi \frac{\partial f}{\partial \boldsymbol{C}} \,\mathrm{d}\boldsymbol{C} = [\phi f]_{U,V,W=-\infty}^{U,V,W=\infty} - \int \frac{\partial \phi}{\partial \boldsymbol{C}} f \,\mathrm{d}\boldsymbol{C} = -n \left\langle \frac{\partial \phi}{\partial \boldsymbol{C}} \right\rangle \tag{41}$$

in which $\phi f \to 0$ as any velocity component approaches $\pm\infty$. By the same argument

$$\int \phi \frac{\partial f}{\partial \boldsymbol{C}} \boldsymbol{C} \,\mathrm{d}\boldsymbol{C} = -n \left\langle \frac{\partial \phi \boldsymbol{C}}{\partial \boldsymbol{C}} \right\rangle = -n\langle \phi \rangle - n \left\langle \frac{\partial \phi}{\partial \boldsymbol{C}} \boldsymbol{C} \right\rangle \tag{42}$$

Using these results, we obtain the Enskog equation, which is a generalization of Maxwell's equation:

$$\begin{aligned}n\mathbb{C}(\phi) = &\frac{Dn\langle \phi \rangle}{Dt} + n\langle \phi \rangle \frac{\partial \langle \boldsymbol{c} \rangle}{\partial \boldsymbol{r}} + \frac{\partial n\langle \phi \boldsymbol{C} \rangle}{\partial \boldsymbol{r}} \\ &- n \left[\left\langle \frac{D\phi}{Dt} \right\rangle + \left\langle \boldsymbol{C} \frac{\partial \phi}{\partial \boldsymbol{r}} \right\rangle + \left\langle \boldsymbol{a} \frac{\partial \phi}{\partial \boldsymbol{C}} \right\rangle \right. \\ &\left. - \frac{D\langle \boldsymbol{c} \rangle}{Dt} \cdot \left\langle \frac{\partial \phi}{\partial \boldsymbol{C}} \right\rangle - \left\langle \frac{\partial \phi}{\partial \boldsymbol{C}} \boldsymbol{C} \right\rangle : \frac{\partial \langle \boldsymbol{c} \rangle}{\partial \boldsymbol{r}} \right]\end{aligned} \tag{43}$$

Setting $\phi = 1$, the mass balance is obtained:

$$\frac{Dn}{Dt} + n \frac{\partial \langle \boldsymbol{c} \rangle}{\partial \boldsymbol{r}} = 0 \tag{44}$$

This equation is also called the equation of continuity, expressing the conservation of the number of particles in the suspension. Inserting the equation of continuity into the Enskog equation (Eq. (43)), simplifies the Enskog equation to

$$\begin{aligned}n\mathbb{C}(\phi) = &n \frac{D\langle \phi \rangle}{Dt} + \frac{\partial n\langle \phi \boldsymbol{C} \rangle}{\partial \boldsymbol{r}} \\ &- n \left[\left\langle \frac{D\phi}{Dt} \right\rangle + \left\langle \boldsymbol{C} \frac{\partial \phi}{\partial \boldsymbol{r}} \right\rangle + \left\langle \boldsymbol{a} \frac{\partial \phi}{\partial \boldsymbol{C}} \right\rangle - \frac{D\langle \boldsymbol{c} \rangle}{Dt} \left\langle \frac{\partial \phi}{\partial \boldsymbol{C}} \right\rangle \right. \\ &\left. - \left\langle \frac{\partial \phi}{\partial \boldsymbol{C}} \boldsymbol{C} \right\rangle : \frac{\partial \langle \boldsymbol{c} \rangle}{\partial \boldsymbol{r}} \right]\end{aligned} \tag{45}$$

With $\phi = \boldsymbol{C}$, this simplified Enskog equation corresponds to the balance of linear momentum:

$$n \frac{D\langle \boldsymbol{c} \rangle}{Dt} + \frac{\partial n\langle \boldsymbol{CC} \rangle}{\partial \boldsymbol{r}} = n\langle \boldsymbol{a} \rangle + n\mathbb{C}(\boldsymbol{C}) \tag{46}$$

because $\langle \boldsymbol{C} \rangle = 0$. The first term denotes the change, following the motion, of momentum. The second term denotes the stress tensor due to particle movement. The first term on the right hand side represent the external body-forces, as fluid influences and gravity. The last term on the right hand side denotes the momentum change due to collisions. The momentum equation and the continuity equation are identical with the equations of continuity and momentum derived for a continuous fluid in hydrodynamics. This provides a justification for the hydrodynamical treatment of a particle suspension.

With $\phi = \boldsymbol{CC}$, the mean of the second moment of velocity fluctuation is obtained from the simplified Enskog equation:

$$\begin{aligned}n \frac{D\langle \boldsymbol{CC} \rangle}{Dt} + \frac{\partial n\langle \boldsymbol{CCC} \rangle}{\partial \boldsymbol{r}} = &-2n\langle \boldsymbol{CC} \rangle : \frac{\partial \langle \boldsymbol{c} \rangle}{\partial \boldsymbol{r}} + 2n\langle \boldsymbol{aC} \rangle \\ &+ n\mathbb{C}(\boldsymbol{CC})\end{aligned} \tag{47}$$

The first term denotes the change of the second moment of velocity fluctuation. The second term represents the third moment of velocity fluctuation. The first term on the right hand side represents the transport of the second moment of velocity fluctuation due to the average velocity of the particles. The second term on the right hand side represents the influence of the external forces. It can be readily seen, that if the force does not depend on $\boldsymbol{C}$, this term vanishes. The last term represents the influences of collisions on the second moment of velocity fluctuation. The balance of third moment of velocity fluctuation is obtained by inserting $\phi = \boldsymbol{CCC}$:

$$n\frac{D\langle \boldsymbol{CCC}\rangle}{Dt} + \frac{\partial n\langle \boldsymbol{CCCC}\rangle}{\partial \boldsymbol{r}} = -3n\langle \boldsymbol{CCC}\rangle : \frac{\partial \langle \boldsymbol{c}\rangle}{\partial \boldsymbol{r}} + 3n\langle \boldsymbol{aCC}\rangle + 3n\langle \boldsymbol{CC}\rangle\langle \boldsymbol{c}\rangle\frac{\partial \langle \boldsymbol{c}\rangle}{\partial \boldsymbol{r}} + n\mathbb{C}(\boldsymbol{CC}) \tag{48}$$

Balances of higher order momenta are fairly easily generated. However, most methods only consider up to second order, and the third order term is closed with a Boussinesq approximation, e.g.

$$\langle \boldsymbol{CCCC}\rangle = -\eta_e \nabla \boldsymbol{CCC} \tag{49}$$

where η_e is the effective viscosity, which can be related to the mean free path of the particles.

In kinetic theory for granular flow, collisions are considered binary and instantaneous. Since only smooth and spherically symmetrical particles are considered, the force which either exerts on the other is directed along the line joining their centers. Moreover, rotation is not considered. It is supposed that the effect of any external force which acts on the particle during collision can be neglected compared to the dynamic effect of the collision. With these assumptions, the velocities before and after a collision have definite values, which are denoted $\boldsymbol{c}_i, \boldsymbol{c}_j$ before the collision, and $\boldsymbol{c}'_i, \boldsymbol{c}'_j$ after the collision. The details of the collision itself are of no importance for the theory; it is only important to know the relation between the initial and the final velocities.

Before the collision, the relative velocity of the two particles is $\boldsymbol{g} \equiv (\boldsymbol{c}_i - \boldsymbol{c}_j)$, and by definition $\boldsymbol{g}\cdot\boldsymbol{n} > 0$ (otherwise the particles move away from each other), where $\boldsymbol{n}$ is the normal unit vector lying in the direction of the vector joining the center of the two particles, defined with its origin at the point of contact (see Fig. 1). The collision impulse $\boldsymbol{P}$ exerted by particle j on particle i is directed along the line connecting the centers,

$$\boldsymbol{P} = m_i(\boldsymbol{c}'_i - \boldsymbol{c}_i) = -m_j(\boldsymbol{c}'_j - \boldsymbol{c}_j) \tag{50}$$

$\boldsymbol{P}$ can be obtained by characterizing the incomplete restitution of the normal component of the relative velocity, using the coefficient of restitution e, with $0 \le e \le 1$:

$$\boldsymbol{g}'\cdot\boldsymbol{n} = -e\boldsymbol{g}\cdot\boldsymbol{n} \tag{51}$$

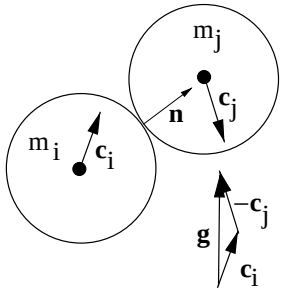

Fig. 1. A pair of colliding particles.

With Eqs. (50) and (51), the equation for $\boldsymbol{P}$ can be derived:

$$\boldsymbol{P} = -\frac{m_i m_j}{m_i + m_j}(1+e)(\boldsymbol{g}\cdot\boldsymbol{n})\boldsymbol{n} \tag{52}$$

Consider the motion of the center of particle j relative to the center of the first particle, i.e. relative to axes moving with the center of particle i (see Fig. 2). For such a collision to occur, the center of particle j must cut a plane through $(\sigma_i + \sigma_j)^2\boldsymbol{n}\,\mathrm{d}\boldsymbol{n}$, where σ_i represents the radius of particle i. Hence, the center of particle j must lie in a volume $(\boldsymbol{g}\,\mathrm{d}t)[(\sigma_i + \sigma_j)^2\boldsymbol{n}\,\mathrm{d}\boldsymbol{n}]$. In a collision between two particles, the value ϕ_j, representing a property of particle j, is changed to ϕ'_j. Thus the particle property ϕ for this particle is changed by the amount $\phi'_j - \phi_j$. The change in $\sum\phi_j$ due to all collisions where particle i has a velocity in $(\boldsymbol{c}_i, \boldsymbol{c}_i + \mathrm{d}\boldsymbol{c}_i)$, particle j has a velocity in $(\boldsymbol{c}_j, \boldsymbol{c}_j + \mathrm{d}\boldsymbol{c}_j)$, occurring in the direction in $(\boldsymbol{n}, \boldsymbol{n} + \mathrm{d}\boldsymbol{n})$, and in time $(t, t + \mathrm{d}t)$ is

$$(\phi'_j - \phi_j) f_{(2)}(\boldsymbol{c}_i, \boldsymbol{r}_i, \boldsymbol{c}_j, \boldsymbol{r}_i + (\sigma_i + \sigma_j)\boldsymbol{n}, t)(\sigma_i + \sigma_j)^2 \times (\boldsymbol{g}\cdot\boldsymbol{n})\,\mathrm{d}\boldsymbol{n}\,\mathrm{d}\boldsymbol{c}_i\,\mathrm{d}\boldsymbol{c}_j\,\mathrm{d}\boldsymbol{r}\,\mathrm{d}t \tag{53}$$

$f_{(2)}(\boldsymbol{c}_i, \boldsymbol{r}_i, \boldsymbol{c}_j, \boldsymbol{r}_j, t)$ represents the pair probability density function, indicating the number density of a pair of particles, where the first particle is located at $\boldsymbol{r}_i$ with velocity $\boldsymbol{c}_i$, and the second particle located at $\boldsymbol{r}_j$ with velocity $\boldsymbol{c}_j$ at time t. $f_{(2)}$ characterizes the statistics of binary collisions.

Integration over all values of $\boldsymbol{c}_1$ and $\boldsymbol{c}_2$ gives the total change during dt in $\sum\phi_i$, summed over all particles in $\mathrm{d}\boldsymbol{r}$, due to collisions. Since the number of particles in $\mathrm{d}\boldsymbol{r}$ is

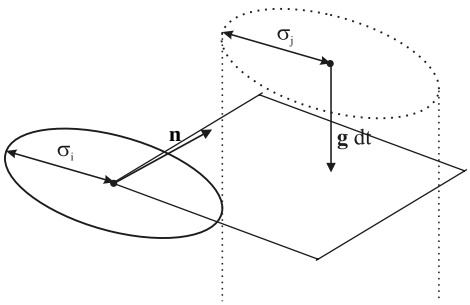

Fig. 2. The outlines of two possible colliding particles. Both particles must lie in a volume $(\boldsymbol{g}\,\mathrm{d}t)[(\sigma_i + \sigma_j)^2\boldsymbol{n}\,\mathrm{d}\boldsymbol{n}]$ to possibly collide.

$n\mathrm{d}\boldsymbol{r}$, this integral must equal $n\mathrm{d}\boldsymbol{r}\mathbb{C}(\phi)dt$. Dividing by $\mathrm{d}\boldsymbol{r}\,\mathrm{d}t$ results in:

$$n\mathbb{C}(\phi)_j = \iiint_{\boldsymbol{g}\cdot\boldsymbol{n}>0} (\phi'_j - \phi_j) f_{(2)}(\boldsymbol{c}_i, \boldsymbol{r}_i, \boldsymbol{c}_j, \boldsymbol{r}_i + (\sigma_i+\sigma_j)\boldsymbol{n}, t)(\sigma_i+\sigma_j)^2(\boldsymbol{g}\cdot\boldsymbol{n})\,\mathrm{d}\boldsymbol{n}\,\mathrm{d}\boldsymbol{c}_i\,\mathrm{d}\boldsymbol{c}_j \quad (54)$$

where the condition $\boldsymbol{g}\cdot\boldsymbol{n} > 0$ indicates that the integration is to be taken over all values of $\boldsymbol{n}$, $\boldsymbol{c}_i$, and $\boldsymbol{c}_2$ for which a collision is impending. For the particle j the rate of increase of property ϕ can be found by the same arguments as above, only by interchanging the roles of the colliding particles by interchanging subscripts i and j and replacing $\boldsymbol{n}$ by $-\boldsymbol{n}$. This contribution may thus be written as

$$n\mathbb{C}(\phi)_i = \iiint_{\boldsymbol{g}\cdot\boldsymbol{n}>0} (\phi'_i - \phi_i) f_{(2)}(\boldsymbol{c}_i, \boldsymbol{r}_j - (\sigma_i+\sigma_j)\boldsymbol{n}, \boldsymbol{c}_j, \boldsymbol{r}_j) \times (\sigma_i+\sigma_j)^2(\boldsymbol{g}\cdot\boldsymbol{n})\,\mathrm{d}\boldsymbol{n}\,\mathrm{d}\boldsymbol{c}_i\,\mathrm{d}\boldsymbol{c}_j \quad (55)$$

In early development of kinetic theory, the pair probability distribution function was expressed as the product of the two individual probability distribution functions:

$$f_{(2)}(\boldsymbol{c}_i, \boldsymbol{r}_i, \boldsymbol{c}_j, \boldsymbol{r}_j, t) \approx f(\boldsymbol{c}_i, \boldsymbol{r}_i, t) f(\boldsymbol{c}_j, \boldsymbol{r}_j, t) \quad (56)$$

This is called the assumption of *molecular chaos*. In the molecular chaos assumption, particles are assumed to be randomly distributed, without their volume playing a role. Hence, particles may overlap. In very dilute systems this may not lead to a large error, as the chance that two particles overlap is very small. For denser gases, Eq. (56) is rewritten as

$$f_{(2)}(\boldsymbol{c}_i, \boldsymbol{r}_i, \boldsymbol{c}_j, \boldsymbol{r}_j, t) \approx g_0 f(\boldsymbol{c}_i, \boldsymbol{r}_i, t) f(\boldsymbol{c}_j, \boldsymbol{r}_j, t) \quad (57)$$

where g_0 is called the radial distribution function at contact. g_0 is equal to one for a dilute particle system, and increases with increasing particle number density, becoming infinite as the particle system approaches the state in which the particles are packed so closely together that motion is impossible. The effect of g_0 is to reduce the volume in which the center of any particle can lie, and so to increase the probability of a collision. By the first assumption of molecular chaos, g_0 is only a function of the position and not a function of the velocity. The function g_0 needs only to be evaluated at the point of contact and not for every position in the system.

The above equation assumes that the two probabilities f_i and f_j are uncorrelated. However, in most practical flows, this will not be the case, but there will be a correlation between the probability density functions of two nearby particles. Simonin and co-workers [22] have researched this influence, and it is not discussed here.

The integrals, Eqs. (54) and (55), are solved by Lun et al. [46] by using the Enskog series expansion [45] and by Jenkins and Richman [47] employing Grads 13 moment system [48]. For the momentum equations, the collisional contribution is written in the form

$$n\mathbb{C}(\phi) = \chi(\phi) - \frac{\partial\Theta(\phi)}{\partial\boldsymbol{r}} - \frac{\partial\langle\boldsymbol{c}\rangle}{\partial\boldsymbol{r}}\Theta\left(\frac{\partial\phi}{\partial\boldsymbol{C}}\right) \quad (58)$$

where Θ is the transfer contribution, due to the transport of ϕ during collision, and χ is a source-like contribution, due to the change of property ϕ during collision. Note that the derivative in the parenthesis of the last term is an argument to the function Θ.

The stress tensor and the flux of fluctuating velocity are

$$\rho\langle\boldsymbol{CC}\rangle = \frac{\rho}{3}\langle C^2\rangle\bar{\bar{I}} - \frac{2\mu}{\eta(2-\eta)g_0}\left[1 + \frac{8}{5}\eta(3\eta-2)\epsilon_s g_0\right]\bar{\bar{D}} \quad (59)$$

$$\frac{1}{2}\rho\langle C^2\boldsymbol{C}\rangle = -\frac{\zeta}{g_0}\left\{\left[1 + \frac{12}{5}\eta^2(4\eta-3)\epsilon_s g_0\right]\nabla\left(\frac{1}{3}\langle C^2\rangle\right) + \frac{12}{5}\eta(2\eta-1)(\eta-1)\frac{d}{d\epsilon_s}(\epsilon_s^2 g_0)\frac{\langle C^2\rangle}{3n}\nabla n\right\} \quad (60)$$

with the abbreviations

$$\zeta = \frac{8\lambda}{\eta(41-33\eta)} \quad (61)$$

$$\lambda = \frac{75m\sqrt{\langle C^2\rangle/3\pi}}{64\sigma^2} \quad (62)$$

$$\eta = \tfrac{1}{2}(1+e) \quad (63)$$

$$\mu = \frac{5m(\langle C^2\rangle/3\pi)}{15\sigma^2} \quad (64)$$

$$\epsilon_s = \frac{nm}{\rho} = \frac{n}{V} \quad (65)$$

$$\bar{\bar{D}} = \tfrac{1}{2}(\nabla\langle\boldsymbol{c}\rangle + \{\nabla\langle\boldsymbol{c}\rangle\}^{\mathrm{T}}) - \tfrac{1}{3}(\nabla\cdot\langle\boldsymbol{c}\rangle)\bar{\bar{I}} \quad (66)$$

For the momentum equation, the source like contribution, χ, is zero, and thus only the transport contribution Θ remains. Thus, the total collisional contribution to the momentum equation has the exact same form as the stress tensor. Therefore, most researchers denote this contribution as 'the collisional contribution to the particle–particle stress'. The term for the momentum equation is

$$\bar{\bar{\Theta}}_{\mathrm{momentum}} \equiv \bar{\bar{P}}_{\mathrm{c}} = \frac{4}{3}\rho\langle C^2\rangle\eta\epsilon_s g_0\bar{\bar{I}} - \frac{16\mu\epsilon_s}{5(2-\eta)}\left[1 + \frac{8}{5}\eta(3\eta-2)\epsilon_s g_0\right]\bar{\bar{D}} - \frac{256}{5\pi}\eta\mu\epsilon_2^2 g_0\left[\frac{6}{5}\bar{\bar{D}} + (\nabla\cdot\langle\boldsymbol{c}\rangle)\bar{\bar{I}}\right] \quad (67)$$

These equations can be directly used to solve the ensemble averaged momentum equations for a granular material, as they can be transformed to the hydrodynamic definitions of viscosities and normal pressure. For the energy equation, both Θ and χ are non-zero. The form of Θ is added in the same form as the flux of fluctuating energy, and is therefore often described as the addition to the flux of fluctuating

energy due to collisions. These terms are

$$\begin{aligned}\boldsymbol{\Theta}_{\text{energy}} \equiv \boldsymbol{q}_{\text{c}} &= -\frac{12\eta\zeta\epsilon_{\text{s}}}{5}\left\{\left[1+\frac{12}{5}\eta^2(4\eta-3)\epsilon_{\text{s}}g_0 + \frac{16}{15\pi}(41-33\eta)\eta\epsilon_{\text{s}}g_0\right]\right.\\ &\quad\times\nabla\left(\frac{1}{3}\langle C^2\rangle\right)\frac{12}{5}\eta(2\eta-1)\\ &\quad\left.\times(\eta-1)\frac{d}{d\epsilon_{\text{s}}}(\epsilon_{\text{s}}^2 g_0)\frac{\langle C^2\rangle}{3n}\nabla n\right\} \qquad (68)\end{aligned}$$

$$\chi_{\text{energy}} = \frac{48}{\sqrt{\pi}}\eta(1-\eta)\frac{\rho\epsilon^2}{\sigma}g_0\left(\frac{\langle C^2\rangle}{3}\right)^{3/2} \qquad (69)$$

Inserting $e = 1$ ($\eta = 1$) into Eq. (69) leads to $\chi = 0$, which shows that the energy equation becomes a conserved quantity for systems where collisions are fully elastic.

A CFD simulation of a dense gas–solid fluidized bed is shown in Fig. 3. This simulation has employed the kinetic theory of granular flow combined with the interphase momentum transfer model of Wen and Yu. It is shown by numerous authors [5,8–10,49–54] that simulations of fluidized beds can give good qualitative prediction.

2.2.3. Dense particle flows

In dense-phase flows, such as fluidized beds, the fluctuating velocity of the fluid phase and its correlation with the properties of particles are negligible compared to particle–particle interactions (collisions and friction) and the mean fluid-particle velocity coupling (drag). Therefore, the fluid phase is often modelled as laminar and fluid property correlations with the fluctuating particle velocities are omitted.

At high solids volume fraction, sustained contacts between particles occur. The resulting frictional stresses must be accounted for in the description of the solid-phase stress. Zhang and Rauenzahn [55] conclude that particle collisions are no longer instantaneous at very high solids volume fractions, as is assumed in kinetic theory. Several approaches have been presented in the literature to model the frictional stress for dense packed particles, mostly originating from geological research groups. Typically, the frictional stress, $\bar{\bar{\sigma}}_{\text{f}}$, is written in an incompressible Newtonian form:

$$\bar{\bar{\sigma}}_{\text{f}} = P_{\text{f}}\bar{\bar{I}} + \mu_{\text{f}}(\nabla\boldsymbol{v} + (\nabla\boldsymbol{v})^{\text{T}}) \qquad (70)$$

The frictional stress is added to the stress predicted by kinetic theory for $\epsilon_{\text{s}} > \epsilon_{\text{s,min}}$:

$$P_{\text{s}} = P_{\text{kinetic}} + P_{\text{f}} \qquad (71)$$

$$\mu_{\text{s}} = \mu_{\text{kinetic}} + \mu_{\text{f}} \qquad (72)$$

Johnson and Jackson [56] propose a semi-empirical equation for the frictional pressure, P_{f}

$$P_{\text{f}} = \text{Fr}\frac{(\epsilon_{\text{s}} - \epsilon_{\text{s,min}})^n}{(\epsilon_{\text{s,max}} - \epsilon_{\text{s}})^p} \qquad (73)$$

where Fr, n, and p are empirical material constants. This expression is valid for $\epsilon_{\text{s}} > \epsilon_{\text{s,min}}$, where $\epsilon_{\text{s,min}}$ is the solids volume fraction at which frictional stresses become important. The order of magnitude of the frictional pressure, with material constants determined by various authors, is shown in Fig. 4. The frictional viscosity is then related to the frictional pressure by the linear law proposed by Coulomb [60],

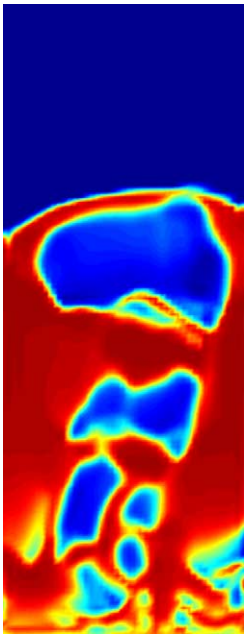

Fig. 3. A snapshot of a transient CFD simulation of a gas–solid fluidized bed. The color indicates the solid volume fraction, red high solids volume fraction, and blue for high gas volume fraction. (For interpretation of the references to color in this figure legend, the reader is referred to the web version of this article.)

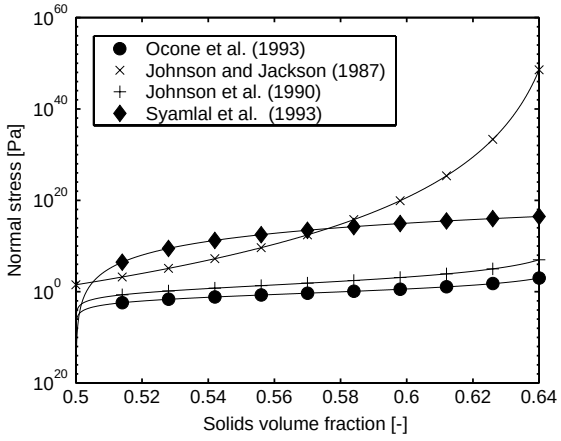

Fig. 4. The normal frictional stress with empirical constants from [57–59].

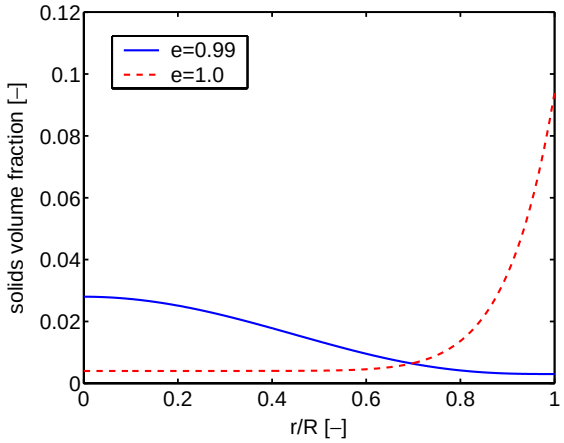

Fig. 5. The axial solids volume fraction profile for 2 values of the particle restitution coefficient.

or Schaeffer [61]:

$$\mu_f = \frac{P_f \sin\phi}{\epsilon_s \sqrt{\begin{array}{l}(1/6)((\partial u_s/\partial x - \partial v_s/\partial y)^2 + (\partial v_s/\partial y)^2 \\ \quad + (\partial u_s/\partial x)^2) + (1/4)(\partial u_s/\partial y + \partial v_s/\partial x)^2\end{array}}} \tag{74}$$

The stresses in the dense regime predicted by frictional stress models are typically much larger than those predicted by kinetic theory. A comparison by Srivastava and Sundaresan [62] shows that the above model is as suitable for dense gas–solid flow as more complex frictional stress models.

2.2.4. Dilute particle flows

The kinetic theory as derived by [46] is able to predict many types of complex gas–solid flows. Sundaresan and co-workers [63], however, showed that this model exhibits a very strong, unrealistic degree of sensitivity to the coefficient of restitution, e. To illustrate this sensitivity, Fig. 5 shows the solids volume fraction in a one dimensional vertical pipe flow for $e = 1$ and 0.99. Although the prediction is fairly good for $e = 1$, as shown in [17], this value of e is unrealistic. Lower values of e give a completely incorrect prediction of the location of the solids in the tube, as was pointed out by [64]. Almstedt and Ljus showed that in horizontal gas–particle pipe-flow, without applying kinetic theory, the modelling results are even worse, leading to that all the solids fall to the bottom of the pipe [19].

One of the important things that are missing to obtain a model suitable for dilute gas–solid flow is gas-phase turbulence. While the magnitude of the gas-phase turbulence is negligible in dense gas–solid flow, it may play a major role in more dilute flows. Several authors have researched the gas-phase turbulence terms, which are present in the diffusion term after closing them with a eddy viscosity model [65,66], and these models were successful in predicting the flow of extremely dilute flows. However, at slightly more dense flows, when the drag between the gas and the solids becomes important, the gas-phase turbulence becomes relatively insignificant and the unrealistic volume fraction contours reappear.

Elgobashi and Abou-Arab [67] performed a Reynolds decomposition of the Eulerian two-fluid equations and found a large number of terms arising from this. Hrenya and Sinclair [64] have modelled three of the time averaged terms arising from this decomposition with the eddy mixing length gradient assumption. They found significant improvement of the results, with solids volume fraction contours similar to experimental data. Although Ljus [19] did not use kinetic theory, they found the same improvement for horizontal pipe-flow.

The type of time-averaging that [19,64] proposed, gives rise to an additional term in the continuity equation. Apart from the problems with numerical scheme this introduces, it also introduces scaling in the eddy viscosity coefficient with the volume fraction. When using Favre averaging instead, the only additional terms arise in the momentum equations. The most important term arises as the correlation between the fluctuating particle velocity and the fluctuating particle volume fraction. When this term is closed with a gradient assumption, this leads to additional dispersion terms in the momentum balance of the order of $\beta\nabla\epsilon$.

Simonin and co-workers [5,14] have used a different expression for the interphase momentum transfer. In their model, they use not the averaged gas velocity as-is, but recognize that the undisturbed local fluid turbulent velocity should be used instead. The differing term, called the turbulent drift velocity [68], can be modelled with a dispersion coefficient and the gradients of the solids and fluid volume fraction. Hence, the form of the dispersive term is the same as obtained from Favre averaging. The advantage with using the turbulent drift velocity is that it gives the order of magnitude of the coefficients in the model, as well as it dependency upon other flow properties.

3. Lagrangian modeling of the dispersed phase

3.1. Fluid–solid modeling

With increasing computer power, discrete particle models, or Lagrangian models, have become a very useful and versatile tool to study the hydrodynamic behavior of particulate flows. In these models, the Newtonian equations of motion are solved for each individual particle, and a collision model is applied to handle particle encounters. Recently, such particle models have been combined with an Eulerian model for the continuous phase to simulate freely bubbling and circulating fluidized beds [25,69–71].

3.1.1. Fluid phase

The motion of the fluid phase is calculated from the averaged fluid-phase governing equations as presented in

Section 2.2.1. The continuity equation for the fluid phase is

$$\frac{\partial \epsilon_g \rho_g}{\partial t} + \nabla \cdot \epsilon_g \boldsymbol{v}_g = 0 \tag{75}$$

and the momentum balance is

$$\frac{\partial \epsilon_g \rho_g \boldsymbol{v}_g}{\partial t} + \nabla(\epsilon_g \rho_g \boldsymbol{v}_g \boldsymbol{v}_g) = -\epsilon_g \nabla P + \epsilon_g \nabla \cdot \bar{\bar{\tau}}_g + \epsilon_g \rho_g \boldsymbol{g} - \frac{\sum_{i=1}^{K} V_{s,i} \beta (\boldsymbol{v}_g - \boldsymbol{v}_{s,i}) \delta(\boldsymbol{x} - \boldsymbol{x}_{s,i})}{\sum_{i=1}^{K} V_{s,i}} \tag{76}$$

where the compressible fluid phase stress tensor is defined as

$$\bar{\bar{\tau}}_g = 2\mu \bar{\bar{D}}_g - \tfrac{2}{3}\mu \,\mathrm{tr}(\bar{\bar{D}}_g)\bar{\bar{I}} \tag{77}$$

where $\bar{\bar{D}}_g$ is the strain rate tensor,

$$\bar{\bar{D}}_g = \tfrac{1}{2}(\nabla \boldsymbol{v}_g + (\nabla \boldsymbol{v}_g)^{\mathrm{T}}) \tag{78}$$

and μ the fluid-phase viscosity.

The last term in Eq. (76) represents the interphase momentum transfer between the fluid phase and each individual particle. δ represents a pulse function, which is one if its argument is zero and zero otherwise. The last term is to ensure that the interphase momentum transfer is only taken into account in the fluid-phase momentum equation at the location of the corresponding particle. As was indicated earlier, a problem of this Lagrangian–Eulerian approach is the length-scale of the averaging. In the Eulerian–Eulerian approach the length scales of the averaged fluid- and particle-phase are equal and the "sub-grid" behavior of the particles is described with the kinetic theory of granular flow. In the Lagrangian–Eulerian approach, the length-scale of the fluid-phase is larger than the length-scale of the particle phase. The information of fluid induced movement of particles, as well as particle induced movement of fluid, cannot be transferred between the phases on the eddy or individual particle scale. Hence, a computational cell in which a small cluster of particles is present is penetrated by the fluid-phase, similar as a fixed porous medium and the fluid phase does not discriminate between homogeneously distributed particles or clustered particles within one cell. In reality, the fluid-phase "dodges" the particle clusters. Particle clustering due to the local fluid flow ("micro-scale" clustering) is thus not captured in the Lagrangian–Eulerian approach. This shortcomings of the outlined model, in the particle–fluid phase coupling, should be well kept in mind when attempting to use this simulation method. So-called "true" direct numerical simulations can be carried out to solve the actual fluid field around each particle (e.g. [72]) but this is extremely computationally expensive and can only be done for a very limited number of particles.

3.1.2. Solid phase

For the solids, we consider flows of inelastic spheres. In a Lagrangian calculation, the path of each individual particle is calculated. The calculation of the paths of the particles consists of two steps: (i) calculation of the particle motion, and (ii) treatment of the collision of a particle with another particle.

The motion of individual particles is completely determined by Newton's second law of motion. The forces acting on each particle, next to collisions, are gravity and the traction force of the fluid phase on the particle. Thus, the momentum equation describing the acceleration of the particle is

$$m_s \boldsymbol{a}_s = m_s \boldsymbol{g} + V_s \nabla \cdot \bar{\bar{\tau}}_g - V_s \nabla P + \beta \frac{V_s}{\epsilon_s}(\boldsymbol{v}_g - \boldsymbol{v}_s) \tag{79}$$

where $\boldsymbol{a}_s$ is the acceleration of one particle, V_s the volume of one particle, P the local pressure, ϵ_s the local solids volume fraction, $\bar{\bar{\tau}}_g$ the fluid phase stress tensor, and β represents the interphase momentum transfer coefficient.

For describing the collisions of particles, two types of approaches are possible, the hard-sphere approach and soft-sphere approach.

3.1.3. Hard-sphere approach

In the hard-sphere approach, collisions between particles are assumed binary and instantaneous. The velocities of the particles emerging from a collision are calculated by considering the balance of linear and angular momenta in the collision. During a collision, energy is stored in elastic deformations associated with both the normal and the tangential displacements of the contact point relative to the center of the sphere. Because the release of this energy may affect the rebound significantly, coefficients of restitution associated with both the normal and tangential components of the velocity at the point of contact are taken into account. This model is employed for both particle–particle and particle–wall collisions.

We consider two colliding spheres with diameters d_1 and d_2, masses m_1 and m_2, and centers located at $\boldsymbol{r}_1$ and $\boldsymbol{r}_2$. The unit normal along the line joining the centers of two spheres is $\boldsymbol{n} = (\boldsymbol{r}_1 - \boldsymbol{r}_2)/|\boldsymbol{r}_1 - \boldsymbol{r}_2|$. During the collision, sphere 2 exerts an impulse $\boldsymbol{J}$ onto sphere 1. Prior to the collision the spheres have translational velocities $\boldsymbol{c}_1$ and $\boldsymbol{c}_2$ and angular velocities $\boldsymbol{\omega}_1$ and $\boldsymbol{\omega}_2$. The corresponding velocities after the collision are denoted by primes. The velocities before and after collision are related by

$$m_1(\boldsymbol{c}_1' - \boldsymbol{c}_1) = -m_2(\boldsymbol{c}_2' - \boldsymbol{c}_2) = \boldsymbol{J} \tag{80}$$

and

$$\frac{2I_1}{d_1}(\boldsymbol{\omega}_1' - \boldsymbol{\omega}_1) = -\frac{2I_2}{d_2}(\boldsymbol{\omega}_2' - \boldsymbol{\omega}_2) = -\boldsymbol{n} \times \boldsymbol{J} \tag{81}$$

where, for example, $I = md^2/10$ is the moment of inertia about the center of a homogeneous sphere. In order to determine the impulse $\boldsymbol{J}$, the relative velocity $\boldsymbol{q}$ at the point of contact is defined:

$$\boldsymbol{q} = (\boldsymbol{c}_1 - \boldsymbol{c}_2) - (\tfrac{1}{2}d_1\boldsymbol{\omega}_1 + \tfrac{1}{2}d_2\boldsymbol{\omega}_2) \times \boldsymbol{n} \tag{82}$$

With the above equations, the contact velocities before and after the collision are given by

$$\boldsymbol{q}'-\boldsymbol{q} = \frac{7}{2}\left(\frac{1}{m_1}+\frac{1}{m_2}\right)\boldsymbol{J} - \frac{5}{2}\left(\frac{1}{m_1}+\frac{1}{m_2}\right)\boldsymbol{n}(\boldsymbol{J}\cdot\boldsymbol{n}) \quad (83)$$

The coefficient of restitution, e, characterizes the incomplete restitution of the normal component of $\boldsymbol{q}$:

$$\boldsymbol{n}\cdot\boldsymbol{q}' = -e\boldsymbol{n}\cdot\boldsymbol{q} \quad (84)$$

where $0 \le e \le 1$. In collisions that involve sliding, the sliding is assumed to be resisted by Coulomb friction and the tangential and normal components of the impulse are related by the coefficient of friction μ:

$$|\boldsymbol{n}\times\boldsymbol{J}| = \mu(\boldsymbol{n}\cdot\boldsymbol{J}) \quad (85)$$

where $\mu \ge 0$. Combining Eqs. (83)–(85) provides an expression for the impulse transfer in the case when the collision is sliding:

$$\boldsymbol{J}^{(1)} = \frac{(1+e)(\boldsymbol{q}\cdot\boldsymbol{n})\boldsymbol{n}+\mu(1+e)\cot\gamma[\boldsymbol{q}-\boldsymbol{n}(\boldsymbol{q}\cdot\boldsymbol{n})]}{1/m_1+1/m_2} \quad (86)$$

where γ is the angle between $\boldsymbol{q}$ and $\boldsymbol{n}$ and the superscript 1 denotes that the collision involves sliding. With small γ the collision is sliding, and as γ increases the sliding stops when

$$\boldsymbol{n}\times\boldsymbol{q}' = -\xi\boldsymbol{n}\times\boldsymbol{q} \quad (87)$$

or equivalently

$$\cot\gamma_0 = \frac{2(1+\xi)}{7(1+e)\mu} \quad (88)$$

where $0 \le \xi \le 1$ is the tangential coefficient of restitution. Collisions with $\gamma \ge \gamma_0$ do not involve sliding but sticking, and in this case the impulse is found by combining Eqs. (83), (84) and (87):

$$\boldsymbol{J}^{(2)} = -\frac{(1+e)(\boldsymbol{q}\cdot\boldsymbol{n})\boldsymbol{n}+(2/7)(1+\xi)[\boldsymbol{q}-\boldsymbol{n}(\boldsymbol{q}\cdot\boldsymbol{n})]}{1/m_1+1/m_2} \quad (89)$$

In this expression, the superscript 2 denotes the collision does not involve sliding, but sticking. The three parameters e, μ, and ξ are taken to be constant and independent of the velocities.

Collisions with a flat wall are treated by considering the wall as a particle with infinite mass and with the appropriate wall values of e, μ, and ξ.

Fig. 6 shows a CFD simulation of a gas fluidized bed employing a hard-sphere model. Various strategies to translate the presence of the two-dimensional "disks" to a three-dimensional volume fraction are compared to each other and with experiments. Although these strategies have been put forward in the literature [69–71], none of them give satisfying results, and three-dimensional simulations are advised here.

3.1.4. Soft-sphere approach

In the soft-sphere approach the particle interactions are modelled through a potential force. This model for contact forces was first proposed by [73]. The physical motivation for the soft-sphere approach is that when two particles collide they actually deform. This deformation, in the soft-sphere model described by the overlap displacement of two particles, is the driving parameter of the force model. The larger the overlap displacement, the larger the repulsive force. In such a particle–particle interaction, the particles lose kinetic energy. When two particles slide under the application of a normal force, a frictional force results. Considering these forces, the soft-sphere model is composed of three mechanical elements, i.e. a spring, dashpot, and friction slider, cf. Fig. 7. The spring simulates the effect of deformation and the dashpot the damping effect. The slider simulates the sliding force between two particles. The effects of these mechanical components on particle motion appear through the following parameters: the stiffness k, the damping coefficient η, and the friction coefficient μ.

The normal component of the forces acting during particle contact is given by the sum of forces modelled by a spring and a dashpot,

$$\boldsymbol{F}_{n,ij} = (-k_{n,ij}\delta_{n,ij} - \eta_{n,ij}\boldsymbol{v}_{\mathrm{r}}\cdot\boldsymbol{n})\boldsymbol{n} \quad (90)$$

where δ is the normal overlap between particles i and j, and $\boldsymbol{v}_{\mathrm{r}}$ is the relative velocity between the two particles. The tangential component of the contact force acting during particle interaction is given by the sum of forces modelled by a spring and a dashpot, or a spring and a slider, depending on the magnitude of the ratio between the normal and tangential component, which physically indicates if a particle is sliding or not.

$$\boldsymbol{F}_{t,ij} = \begin{cases} -k_{t,ij}\delta - \eta_{t,ij}\boldsymbol{J}_{ij}, & |-k_{t,ij}\delta-\eta_{t,ij}| \le \mu|\boldsymbol{F}_{n,ij}| \\ -\mu|\boldsymbol{F}_{n,ij}|\dfrac{\boldsymbol{J}_{ij}}{|\boldsymbol{J}_{ij}|}, & |-k_{t,ij}\delta-\eta_{t,ij}| > \mu|\boldsymbol{F}_{n,ij}| \end{cases} \quad (91)$$

where $\boldsymbol{J}_{ij}$ is the slip velocity at the point of contact and μ is the friction coefficient which indicates when the interaction between to particles is considered sliding. The force on each particle in the system consists out of the above normal and tangential forces caused by the respective particle overlap.

The stiffness coefficient k and the damping coefficient η may be related to physical particle properties by means of Hertzian contact theory [25] and the displacement theory of Mindlin and Deresiewicz [74].

The time-step which can be taken in hard-sphere collision dynamics is governed by the successive time between collisions. In dense systems this time-step may be very small, leading to very long computational times. The time-step in soft-sphere collision dynamics is governed by the stiffness of the normal and tangential forces. Unfortunately, the Hertzian contact theory predicts such high stiffness that in practical

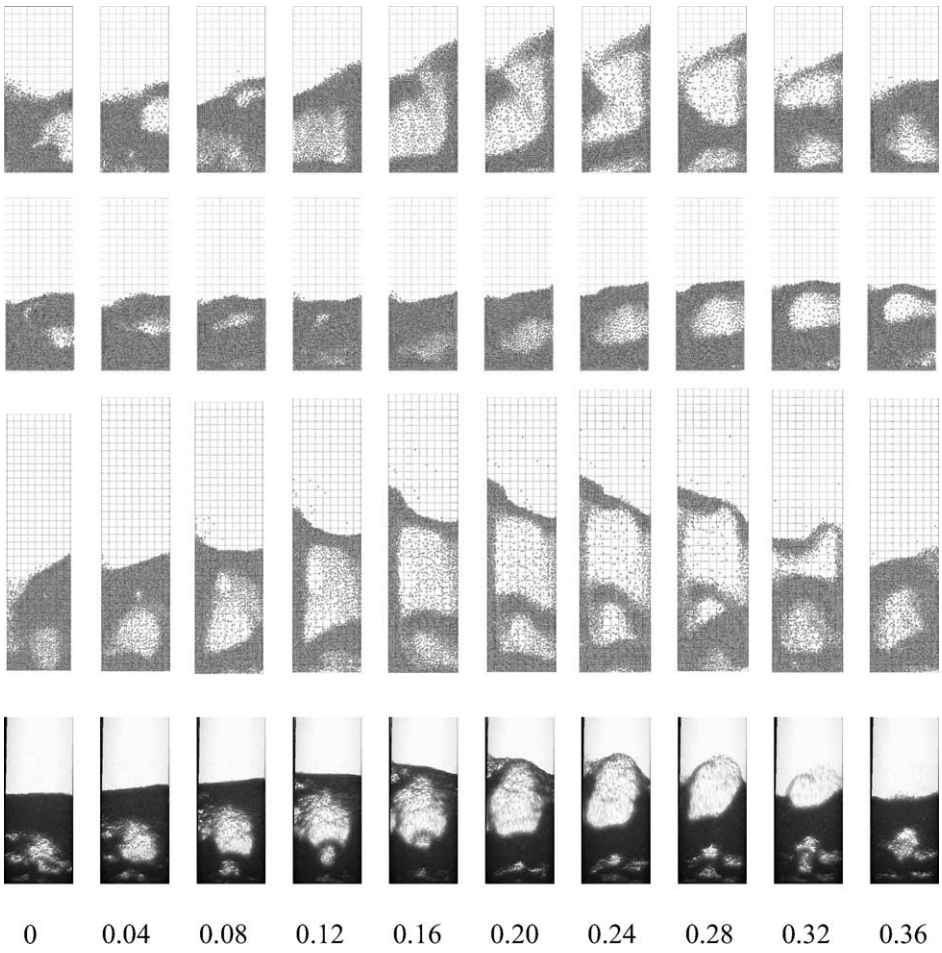

Fig. 6. Ten snapshots of a visual representation of the location of the particles at equidistant times (given at the bottom of the series in 's') at a superficial gas velocity of $U = 0.9$ m/s. The three series on the top are simulations with different strategies to translate the presence of the two-dimensional particles to a three-dimensional volume fraction, and the series at the bottom is an experimental result. For details, see [71].

cases this also leads to very small possible time-steps in denser suspensions. Tsuji et al. [25] have suggested to use a lower value for the stiffness coefficient. According to [25,75,76], the physical impact of this is low, but the exact meaning or limits of this are unknown.

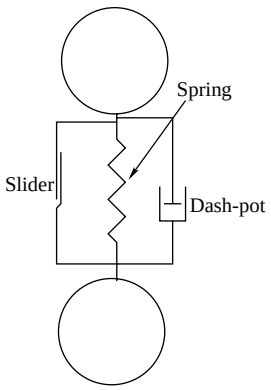

Fig. 7. A spring–damper–dashpot system to model particle contact.

4. Interface tracking methods

When studying the behaviour of a relatively small number of interfaces, for instance to study a few droplets or bubbles in a fluid–fluid flow, methods which track the location of the interface can be applied. One of the most well-known methods is the volume-of-fluid method [26]. In the VOF method, the fluid location is recorded by employing a volume-of-fluid function, or color function, which is defined as unity within the fluid regions and zero elsewhere, hence representing the local volume fraction of one of the phases. In practical numerical simulations employing a VOF algorithm, this function is unity in computational cells occupied completely by fluid of phase 1, zero in regions occupied completely by phase 2, and a value between these limits in cells which contain a free surface. In the VOF algorithm, the color function is discontinuous over the interface. In the closely related level-set algorithm, a color function is also employed, but this function is continuous and having no direct physical meaning. The local volume fraction is translated from the local value or gradient of the color function.

An advantage of the level-set algorithm is its simplicity to compute derivatives of the color function, required for instance to calculate the curvature of the surface. A disadvantage of this approach, is that the numerical representation of the transport equation to determine the values of the color function is prone to numerical error and leads to a loss or gain of mass when calculating the local volume fractions. Successful implementations of the level-set methods have been demonstrated, for instance, by [27,28]. However, simulations of gas/liquid systems using this method have not been validated experimentally yet.

In VOF methods, the color function is a semi-discontinuous function, facilitating the calculation of the properties of each of the phases and making it possible to present an accurate numerical scheme for solving the color transport equation. However, the accurate calculation of the curvature of the interface, by determining the derivative of the color function, is difficult from a numerical point of view.

Recently, significant progress has been made in the numerics and application of the VOF and level-set algorithms, e.g. [77,78]. However, there is very little experimental validation to verify VOF or level-set simulation results. Moreover, when employing the VOF algorithm, it is still difficult to obtain a good estimate of the curvature of the free surface.

A separate class of methods are the so-called front tracking methods [79,31] where fictitious particles are placed along the interface. The particles move with the fluid and the interface is reconstructed from the location of the particles.

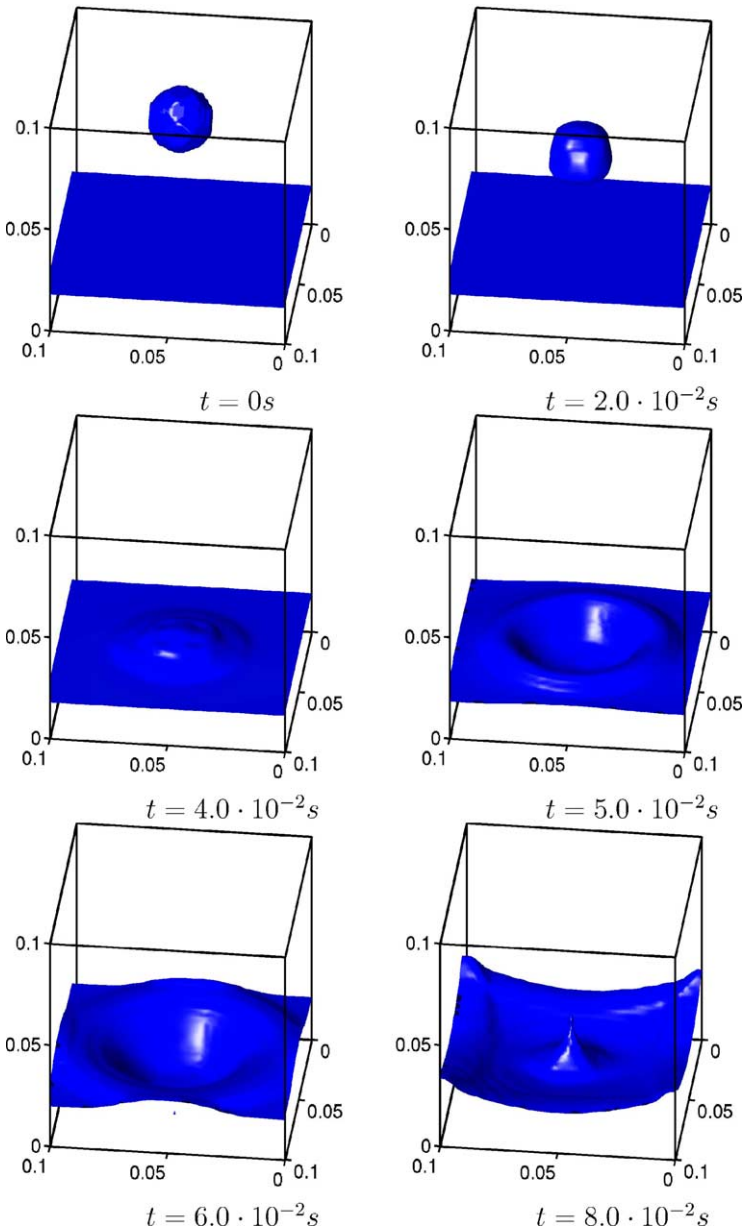

Fig. 8. The simulation of a droplet falling upon a liquid layer in a box with hydrophobic walls. Units are in metre. For details, see [30].

The results are reported to be accurate, but expensive. Also, the reconstruction of the interface can be troublesome, especially when break-up or coalescence of the interface occurs. Then, this method needs to be combined with another method to produce accurate results [31].

All interface tracking methods consider two separate, incompressible fluid phases. The two phases are separated by a reconstructed interface, from some color function or another Lagrangian representation of the interface. The Navier–Stokes equation for the incompressible fluid phases reads

$$\rho\frac{\partial \boldsymbol{u}}{\partial t} + \rho\nabla(\boldsymbol{u}\boldsymbol{u}) = -\nabla P + \nabla\cdot\bar{\bar{\tau}} + \rho\boldsymbol{g} + \boldsymbol{S} \tag{92}$$

with the continuity equation for an incompressible fluid,

$$\nabla\cdot\boldsymbol{u} = 0 \tag{93}$$

where ρ is the density of the local fluid, P the local pressure, $\boldsymbol{S}$ the surface tension, $\bar{\bar{\tau}}$ the viscous stress tensor, and $\boldsymbol{u}$ the velocity field. The velocity field holds both the liquid and the gas velocity. Viscosity and density are assumed constant in each of the phases, but may vary from phase to phase, with values ρ_i and μ_i for phase i.

In the standard VOF or set-level methods, a transport equation to determine the evolution of the color function is solved [26]

$$\frac{\partial \xi}{\partial t} + \boldsymbol{u}\cdot\nabla\xi = 0 \tag{94}$$

in which ξ is represented as a color function, denoting either phase 1 or phase 2. In the level-set method the scalar ξ is a smooth function, and in the VOF method ξ represents the local volume fraction of phase 1.

The first VOF type approach was suggested by [26]. Although this scheme is still often applied, it performs badly on the Rudman translation test [80], in which the fluid is translated diagonally over the mesh, and the Rider–Kothe reversed single vortex test [81], in which the fluid is conservedly rotated. Also other piecewise constant schemes (e.g. [82]) show a large amount of smearing of the interface and a violation of the conservation of each of the phases [77]. The application of so-called surface sharpening models, as present in some commercial CFD codes, can somewhat prevent the smearing of the interface.

Piecewise linear schemes are able to track a linear surface, including its orientation. Youngs's VOF method [83] and the stream scheme [84] are examples of these. This piecewise linear profile obtained from these methods more closely represents the actual interface geometry. These schemes are much more complex then piecewise constant schemes, especially in three dimensions, but they have been shown to be significantly more accurate in numerical tests [30,80,81,84]. An example of a falling and colliding droplet calculated with a Lagrangian piecewise linear method is shown in Fig. 8.

5. Discussion and conclusion

This article provides an overview of physical models and closures employed for computational fluid dynamic predictions of multiphase flows. A separate description is given of the Eulerian framework and the Lagrangian framework. Also, a separate class of multiphase CFD models are discussed, namely the interface tracking methods.

Concerning the Eulerian framework, we have compared the different formulations for fluid–fluid flow and fluid–solid flow. The differences between these formulations lie in the fact that the points inside one particle are fully correlated to each other unlike in a fluid droplet or bubble. For applications where the gradient of the volume fraction is expected to be small, the differences are minor. However, when the gradient of the volume fraction plays an important role, for instance in cluster formation in dilute flows, it is believed that the two formulations will quantitatively differ.

A number of important closures are required in the Eulerian framework for fluid–fluid flow. These are often not accurate at high dispersed phase volume fractions. On some of the closures, there is even a dispute on their formulation, while others are difficult to implement numerically.

For the fluid–solid Eulerian closure models this article explains the kinetic theory starting, from first principles by deriving the Boltzmann and Enskog equations. The resulting equations give a powerful basis to implement further closure models, for example, for fluid phase turbulence interactions with the particles. A particle collision model is employed taking into account the inelastic nature of particles, but neglecting the particle rotation. The probability correlation between two colliding particles due to the flow of the fluid is neglected, but it is expected that this is an important phenomenon, especially in dilute flows where the fluid phase plays a dominant role. The final closures arising from the kinetic theory of granular flow are presented, which have been used with a fair amount of success in fluid–solid calculations. Also, a short discussion is given of physical features arising from dilute and dense flows.

In the Lagrangian framework, two common methods are used in fluid–solid modelling: i.e. the hard-sphere approach and the soft-sphere approach. In the hard-sphere approach, particle collisions are assumed binary and instantaneous, like the collision between to billiard balls. This might be an appropriate model for dilute flows, but for dense flows collisions are far from binary and instantaneous. An alternative to the hard-sphere approach, is the soft-sphere approach, where particles can overlap and particle interactions can be enduring. This is modelled by a slider–spring–dashpot model, with associated friction, spring, and damping coefficients. When employing physical values for these coefficients, unfortunately, the equations become stiff and numerically hard to solve.

Interface tracking methods, of which the volume-of-fluid model is the most common in multiphase flow, can be employed to study the behaviour of a small number of

interfaces. The idea behind these interface tracking methods is that the same set of equations is solved for predicting the evolution of both fluid phases, the Navier–Stokes equations. Next to solving the Navier–Stokes equations, with a viscosity and density which can locally vary due to the local fluid, an equation for the interphase is solved. There are different ways formulating and solving this equation. Interface tracking methods can be used with a reasonable degree of success, depending upon the problem, the type of interface method, and the accuracy of the underlying numerics.

From this review it has hopefully become apparent that the application of multiphase CFD is very promising but requires further development.

Acknowledgements

Berend van Wachem is a former Ph.D. student of C.M. van den Bleek and has received excellent guidance during his Ph.D. studies from him. Berend has enjoyed the many formal and informal discussions on multiphase flows, the modelling of multiphase flows and a variety of other subjects. Alf-Erik Almstedt would like to thank Cor van den Bleek for many years of pleasant informal collaboration and for recommending one of his top students, Berend van Wachem, to the position as associate professor in the multiphase flow group at Chalmers.

References

[1] T. Anderson, R. Jackson, A fluid mechanical description of fluidized beds, Ind. Eng. Chem. Fundam. 6 (4) (1967) 527–539.
[2] S. Garg, J. Pritchett, Dynamics of gas-fluidized beds, J. Appl. Phys. 46 (10) (1975) 4493–4500.
[3] J. Pritchett, T. Blake, S. Garg, A numerical model of gas fluidized beds, AIChE Symp. Ser. 74 (176) (1978) 134–148.
[4] G. Balzer, O. Simonin, Extention of eulerian gas–solid flow modelling to dense fluidized bed, in: P. Viollet (Ed.), Proceedings of the 5th International Symposium on Refined Flow Modelling and Turbulence Measurements, France, Paris, 1993, pp. 417–424.
[5] G. Balzer, O. Simonin, A. Boelle, J.L. Vieville, A unifying modelling approach for the numerical prediction of dilute and dense gas–solid two phase flow, in: 5th international conference on circulating fluidized beds, 1996.
[6] A. Boemer, H. Qi, U. Renz, Eulerian simulation of bubble formation at a jet in a two dimensional fluidized bed, Int. J. Multiphase Flow 23 (1997) 927–944.
[7] J. Ding, D. Gidaspow, A bubbling fluidization model using theory of granular flow, AIChE J. 36 (4) (1990) 523–538.
[8] J. Ding, R. Lyczkowski, Three-dimensional kinetic theory modeling of hydrodynamics and erosion in fluidized beds, Powder Technol. 73 (1992) 127–138.
[9] H. Enwald, E. Peirano, A. Almstedt, Eulerian two-phase flow theory applied to fluidization, Int. J. Multiphase Flow 22 (1996) 21–66.
[10] G. Ferschneider, P. Mege, Eulerian simulation of dense phase fluidized beds, Institut Francais du Petrole, BP 3, 69390 Vernaison, France, 1995.
[11] D. Gidaspow, Y. Seo, B. Ettehadieh, Hydrodynamics of fluidization: experimental and theoretical bubble sizes in a two-dimensional bed with a jet, Chem. Eng. Commun. 22 (1983) 253–272.
[12] D. Gidaspow, Multiphase Flow and Fluidization, first ed., Academic Press, San Diego, 1994.
[13] J. Kuipers, A two-fluid micro balance model of fluidized beds, Ph.D. Thesis, University of Twente, The Netherlands, 1990.
[14] J. Lavieville, E. Deutsch, O. Simonin, Large eddy simulation of interactions between colliding particles and a homogeneous isotropic turbulence field, in: ASME Meeting on Gas–Solid Flows, FED, vol. 228.
[15] C. Lun, S. Savage, The effects of an impact velocity dependent coefficient of restitution on stresses developed by sheared granular materials, Acta Mech. 63 (1986) 15–44.
[16] P. Nott, Analysis of granular flow in aerated and vibrated chutes, Ph.D. Thesis, Princeton University, Princeton, 1991.
[17] J. Sinclair, R. Jackson, Gas–particle flow in a vertical pipe with particle–particle interactions, AIChE J. 35 (1989) 1473.
[18] M. Syamlal, A review of granular stress constitutive relations, US Department of Energy, DOE/MC/21353-2372, DE87006499, 1987, pp. 1–23.
[19] C. Ljus, On Particle Transport and Turbulence Modification in air-particle flows, Ph.D. Thesis, Chalmers University of Technology, Göteborg, Sweden, 2000.
[20] B. van Wachem, J. Schouten, R. Krishna, C.V. den Bleek, J. Sinclair, Comparative analysis of CFD models of dense gas–solid systems, AIChE J. 46 (2001) 1035–1051.
[21] M. Ishii, Thermo-fluid dynamic theory of two-phase flow, Direction des Etudes et Recherches d'Electricité de France, Eyrolles, Paris, France, 1975.
[22] A. Boelle, G. Balzer, O. Simonin, Second order prediction of the particle phase stress tensor of inelastic spheres in simple shear dense suspensions, gas–particle flows, ASME FED 228 (1995) 9–18.
[23] M. Louge, J. Jenkins, M. Hopkins, Computer simulations of rapid granular shear flows between parallel bumpy boundaries, Phys. Fluids A 2 (1990) 1042–1044.
[24] M. Louge, Computer simulations of rapid granular flows of spheres interacting with a flat, frictional boundary, Phys. Fluids 6 (1994) 2253–2269.
[25] Y. Tsuji, T. Kawaguchi, T. Tanaka, Discrete particle simulation of two-dimensional fluidized bed, Powder Technol. 77 (1993) 79–87.
[26] C. Hirt, B. Nicholls, Volume of fluid (VOF) method for the dynamics of free boundaries, J. Comp. Phys. 39 (1981) 201.
[27] B. Koren, A. Venis, A fed back level-set method for moving material–void interfaces, J. Comp. Appl. Math 101 (1999) 131–152.
[28] M. Sussman, P. Smereka, S. Osher, A level set approach for computing solutions to incompressible two-phase flow, J. Comput. Phys. 114 (1994) 146.
[29] D. Gueyffier, J. Li, R. Scardovelli, S. Zaleski, Volume-of-fluid interface tracking with smoothed surface stress methods for three-dimensional flows, J. Comp. Phys. 152 (1999) 423–456.
[30] B. van Wachem, J. Schouten, Experimental validation of 3-D lagrangian VOF model: bubble shape and rise velocity, AIChE J. 48 (2002) 2744–2753.
[31] D. Enright, R. Fedkiw, J. Ferziger, I. Mitchell, A hybrid particle level set method for improved interface capturing, in: Computational Mathematics Program, Scientific Computing Group, Stanford University, 2001.
[32] M. Ishii, K. Mishima, Two-fluid model and hydrodynamic constitutive relations, Nucl. Eng. Des. 82 (1984) 107–126.
[33] J. Dalla Valle, Micromeritics, Pitman, London, 1948.
[34] D. Lathouwers, Modelling and simulation of turbulent bubbly flow, Ph.D. Thesis, Delft University of Technology, The Netherlands, 1999.
[35] H. Lamb, Hydrodynamics, Cambridge University Press, Cambridge, 1932.
[36] D. Drew, R. Lahey, Particulate Two-Phase Flow, Butterworth-Heinemann, Boston, 1993, Chapter 16, pp. 509–566.
[37] A. Tomiyama, H. Tamai, I. Zun, S. Hosokawa, Transverse migration of single bubbles in simple shear flows, Chem. Eng. Sci. 57 (2002) 1849–1858.

[38] R. Jackson, Locally averaged equations of motion for a mixture of identical spherical particles and a newtonian fluid, Chem. Eng. Sci. 52 (1997) 2457–2469.
[39] R. Jackson, Erratum, Chem. Eng. Sci. 53 (1998) 1955.
[40] A. Nadim, H. Stone, The motion of small particles and droplets in quadratic flows, Stud. Appl. Mech. 85 (1991) 53–73.
[41] J. Garside, M. Al-Dibouni, Velocity–voidage relationship for fluidization and sedimentation, I&EC Proc. Des. Dev. 16 (1977) 206–214.
[42] J. Richardson, W. Zaki, Sedimentation and fluidisation. Part I, Trans. Inst. Chem. Eng. 32 (1954) 35–52.
[43] S. Ergun, Fluid flow through packed columns, Chem. Eng. Prog. 48 (1952) 89–94.
[44] C. Wen, Y. Yu, Mechanics of fluidization, Chem. Eng. Prog. Symp. Ser. 62 (1966) 100–111.
[45] S. Chapman, T. Cowling, The Mathematical Theory of Non-Uniform Gases, third ed., Cambridge University Press, Cambridge, 1970.
[46] C. Lun, S. Savage, D. Jefferey, N. Chepurniy, Kinetic theories for granular flow: inelastic particles in couette flow and slightly inelastic particles in a general flowfield, J. Fluid Mech. 140 (1984) 223–256.
[47] J. Jenkins, M. Richman, Grad's 13-moment system for a dense gas of inleastic spheres, Arch. Ration. Mech. Anal. 87 (1985) 355–377.
[48] H. Grad, Asymptotic theory of the boltzmann equation, Phys. Fluids 6.
[49] H. Enwald, A. Almstedt, Fluid dynamics of a pressurized fluidized bed: comparison between numerical solutions from two-fluid models and experimental results, Chem. Eng. Sci. 54 (1999) 329–342.
[50] G. Balzer, A. Boelle, O. Simonin, Eulerian gas–solid flow modelling of dense fluidized bed, in: Proceedings of Fluidization VIII, International Symposium of the Engineering Foundation, 1995, pp. 1125–1134.
[51] A. Boemer, H. Qi, U. Renz, S. Vasquez, F. Boysan, Eulerian computation of fluidized bed hydrodynamics—a comparison of physical models, in: Proceedings of the 13th International Conference on FBC, Orlando, USA, 1995, pp. 775–786.
[52] B. van Wachem, J. Schouten, R. Krishna, C.V. den Bleek, J. Sinclair, Comparative analysis of CFD models of dense gas–solid systems, AIChE J. 47 (2001) 1035–1051.
[53] B. van Wachem, J. Schouten, R. Krishna, C.V. den Bleek, Eulerian simulations of bubbling behaviour in gas–solid fluidised beds, Comput. Chem. Eng. 22 (1998) s299–s306.
[54] B. van Wachem, J. Schouten, R. Krishna, C.V. den Bleek, Validation of the Eulerian simulated dyanmic behaviour of gas–solid fluidised beds, Chem. Eng. Sci. 54 (1999) 2141–2149.
[55] D. Zhang, R. Rauenzahn, A viscoelastic model for dense granular flows, J. Rheol. 41 (1997) 1275–1298.
[56] P. Johnson, R. Jackson, Frictional–collisional constitutive relations for granular materials, with application to plane shearing, J. Fluid Mech. 176 (1987) 67–93.
[57] R. Ocone, S. Sundaresan, R. Jackson, Gas–particle flow in a duct of arbitrary inclination with particle–particle interactions, AIChE J. 39 (1993) 1261–1271.
[58] P. Johnson, P. Nott, R. Jackson, Frictional–collisional equations of motion for particulate flows and their application to chutes, J. Fluid Mech. 210 (1990) 501–535.
[59] M. Syamlal, W. Rogers, T. O'Brien, Mfix Documentation Theory Guide, US Department of Energy, Office of Fossil Energy DOE/METC-94/1004(DE94000087) (Technical note).
[60] C. Coulomb, Essai sur une application des règles de maximis et minimis à quelques problèmes de statique, relatifs à l'architecture, Acad. R. Sci. Mém. Math, Phys. par Divers Savants 7 (1776) 343–382.
[61] D. Schaeffer, Instability in the evolution equations describing incompressible granular flow, J. Differ. Equat. 66 (1987) 19–50.
[62] A. Srivastava, S. Sundaresan, Analysis of a frictional-kinetic model for gas–particle flow, Powder Technol. 129 (2003) 72–85.
[63] J. Pita, S. Sundaresan, gas–solid flow in vertical tubes, AIChE Symp. Ser. 37 (7) (1991) 1009–1018.
[64] C. Hrenya, J. Sinclair, Effects of particle-phase turbulence in gas–solid flows, AIChE J. 43 (1997) 853–869.
[65] M. Louge, E. Mastorakos, J. Jenkins, The role of particle collisions in pneumatic transport, J. Fluid Mech. 231 (1991) 345–359.
[66] E. Bolio, J. Yashuna, J. Sinclair, Dilute turbulent gas–solid flow in risers with particle–particle interactions, AIChE J. 41 (6) (1995) 1375–1388.
[67] S. Elgobashi, T. Abou-Arab, Two-equation turbulence model for two-phase flows, Phys. Fluids 26 (4) (1983) 931–938.
[68] E. Deutsch, O. Simonin, Large eddy simulation applied to the motion of particles in stationary homogeneous turbulence, Tubulence modification in multiphase flow, ASME FED 1 (1991) 34–42.
[69] B. Hoomans, J. Kuipers, W. Briels, W. van Swaaij, Discrete particle simulation of bubble and slug formation in a two-dimensional gas-fluidised bed: A hard-sphere approach, Chem. Eng. Sci. 51 (1) (1996) 99–118.
[70] B. Xu, A. Yu, Numerical simulation of the gas–solid flow in a fluidized bed by combining discrete particle method with computational fluid dynamics, Chem. Eng. Sci. 52 (16) (1997) 2785–2809.
[71] B. van Wachem, J. van der Schaaf, J. Schouten, R. Krishna, C. de Bleek, Experimental validation of lagrangian-eulerian simulation of fluidized beds, Powder Technol. 116 (2001) 155–165.
[72] H. Hu, Direct simulation of flows of solid–liquid mixtures, Int. J. Multiphase Flow 22 (2) (1996) 335–352.
[73] P. Cundall, O. Strack, A discrete numerical method for granular assemblies, Geotechnique 29 (1979) 47.
[74] R. Mindlin, H. Deresiewicz, Elastic spheres in contact under varying oblique forces, J. Appl. Mech. 20 (1953) 327–344.
[75] B. Hoomans, Granular dynamics of gas–solid two-phase flows, Ph.D. Thesis, Twente University of Technology, 2000.
[76] C. Crowe, M. Sommerfeld, Y. Tsuji, Multiphase flows with droplets and particles, CRC Press, Boca Raton, 1998.
[77] D. Kothe, W. Rider, Comment on modeling interfacial flows with volume-of-fluid methods, Tech. Rep. LA-UR-3384, Los Alamos National Laboratory, 1995 (http://public.lanl.gov/mww/HomePage.html).
[78] M. Sussman, E. Puckett, A coupled level set and volume-of-fluid method for computing—3d and axisymmetric incompressible two-phase flows, J. Comput. Phys. 162 (2000) 301–337.
[79] S. Unverdi, G. Tryggvason, A front-tracking method for viscous, incompressible, multi-fluid flows, J. Comp. Phys. 100 (1993) 25–37.
[80] M. Rudman, Volume-tracking methods for interfacial flow calculations, Int. J. Num. Methods Fluids 24 (1997) 671.
[81] W. Rider, D. Kothe, Reconstructing volume tracking, J. Comp. Phys. 141 (1998) 112–152.
[82] B. Lafaurie, C. Nardone, R. Scardovelli, S. Zaleski, G. Zanetti, Modelling merging and fragmentation in multiphase flows with surfer, J. Comp. Phys. 113 (1993) 134–147.
[83] D. Youngs, Time-dependent multimaterial flow with large fluid distortion, in: K. Morton, M. Baines (Eds.), Numerical methods for fluid dynamics, Academic Press, New York, 1982, pp. 273–285.
[84] D. Harvie, D. Fletcher, A new volume of fluid advection algorithm: the stream scheme, J. Comput. Phys. 162 (2000) 1–32.